

Wave loads on cylinders

by

P. Frigaard, Ph.D. student

and

H.F. Burcharth, Professor of Marine Civil Engineering

University of Aalborg
Department of Civil Engineering
Sohngaardsholmsvej 57, DK-9000 Aalborg, Denmark

1 Introduction

Wave loads may be defined as time varying forces on a body resulting from the wave induced flow field which surrounds the body in whole or in part. Such unsteady fluid forces are the net result of the pressure and shear forces integrated over the instantaneous wetted area.

This note deals only with cylinders where the diameter - wave length ratio is small enough to neglect diffraction effects.

The main problem when trying to calculate wave loads is that wave forces are dependent not only of the instantaneous free flow velocity, but also depend of the history of the flow field. This is illustrated in Fig. 1, which shows a circular cylinder in impulsively started flow, i.e. flow suddenly accelerated to a constant unidirectional flow velocity U_0 at time t_{U_0} .

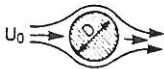




| | | |
|---|--|--|
|  | $t_1 = t_{U_0}$ symmetric flow as found from potential theory | Reynolds number for the similar flow fields generated in normal stationary flow around smooth cylinder |
|  | $t_2 > t_1$ separation in boundary layer | $Re \simeq 10$ |
|  | $t_3 > t_2$ fixed pair of vortices in wake | $Re \simeq 20$ |
|  | $t_4 > t_3$ asymmetric vortex shedding | $Re \simeq 300$ |
|  | $t_5 > t_4$ narrow vortex wake | $Re \sim 3 \cdot 10^5$ |

Figure 1: *Flow field around circular cylinder in impulsively started water flow reaching a constant free stream velocity U_0 .*

In the initial situation the flow field is similar to the flow field found from potential theory.

As time goes by separation starts and a pair of fixed vortices is formed behind the cylinder. Shortly after separation takes place in a single mobile point creating an alternating vortex street. At this stage the *flow force will be time varying in size and direction* although the free stream is stationary, see also Fig. 2.

Later on the onset of turbulent boundary layer the separation point moves backwards and the vortex shedding is disorganized with a broad band of shedding frequencies. The narrowing of the leeside under pressure zone creates a drop in the drag.

It follows from Fig. 1 that even in a unidirectional flow situation the hydrodynamic forces on a cylinder are generally speaking dependent on the historical development of the flow field. In oscillatory and wavy flows the situation is even more complex mainly due to reversal of the wake and the possible changes of the boundary layer from laminar to turbulent. This explains the problems of estimating the wave forces on cylinders.

Nevertheless, hydrodynamic forces on any body in every situation may be calculated using the Navier-Stokes equation and the equation of continuity when boundary conditions are known. The limitation is only given by the capacity of today's computers being too small, but there is no doubt that, in the future, numerical

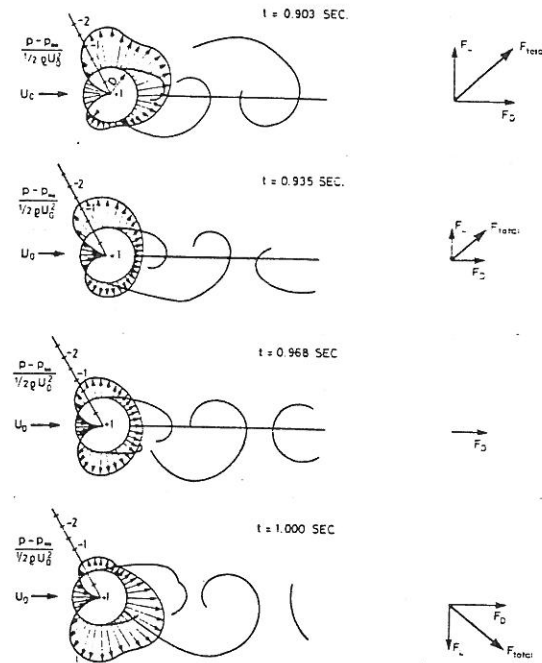


Figure 2: Example of wake formation and measured surface pressure in steady flow (Blevins 1977).

methods based on the Navier-Stokes equation will be more and more predominant. However, due to the complexity and extent of calculating the hydrodynamic forces by discretising the problem, the todays standard of using semiempirical formulae will proceed as praxis in many years.

Since 1950 the calculations of wave forces on cylinders have been based on Morison's equation. Morison's equation for the in-line horizontal force per unit length on a vertical cylinder represents the total force as the sum of a linear inertial component and a non-linear drag component. For a cylinder of diameter D in a flow normal to the axis with free stream velocity and acceleration \dot{u} the equation reads

$$F = C_m \cdot \rho \cdot \pi \cdot D^2/4 \cdot \dot{u} + C_d \cdot \rho \cdot D/2 \cdot u \cdot |u| \quad (1)$$

ρ being the density of sea-water, C_m and C_d being Morison's inertia and drag coefficients.

As is very well known much experimental work has been carried out to obtain values of the C_m and C_d coefficients. The experiments have been done on models of piles in laboratory wave flumes, bassins, and oscillatory water tunnels and a number of prototype field measurements have been performed. Many extensions of Morison's equation have been proposed in order to deal with importance of roughness, rotation of the velocity vector, orientation of the cylinder, proximity of other elements, shadow effects, spanwise correlation, currents, free surface effects, short-crestness of sea etc.

The objective of this note is to discuss the Morison coefficients in all these

situations. But in order to give a physical understanding of the equation we will discuss the inertia term and the drag term.

2 The Froude-Krylov force and added mass.- (Inertia term)

The inertia force can be treated in two parts. One representing the pressure on the cylinder from the non-distributed wave (the Froude-Krylov force), and one representing the extra force caused by the change in pressure due to the presence of the cylinder.

Fig. 3 shows a cylinder with diameter D placed in water depth d , and we want to find the wave force F per unit length of the cylinder.

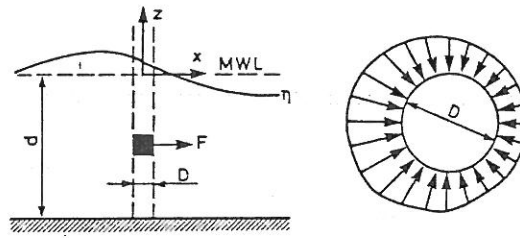


Figure 3: Sketch of 'liquid' cylinder in water.

When looking at the resulting pressure on the 'liquid' cylinder it should be noted that this pressure corresponds to a force able to give the liquid mass $M = \rho \cdot \pi \cdot D^2/4$ the undisturbed horizontal acceleration \dot{u} . When the diameter D is much smaller than the wavelength L , so that the pressure gradient and the acceleration are almost constant across the 'liquid' cylinder, Newton's 2. law (*Force = mass · acceleration*) can be applied to obtain

$$F_{FK} = \rho \cdot \pi \cdot D^2/4 \cdot \dot{u} = m \cdot \dot{u} \quad (2)$$

The index FK means 'Froude-Krylov'. The acceleration might be considered constant over the cylinder when $L/D > 5$.

The cylinder disturbs the flow field in the area around the cylinder. This of cause will change the pressures in the flow, and thereby the resultant force. For streamline bodies like ships etc. the change in the flowfield is moderate in which case the Froude-Krylov force is a good estimate on the total force.

For small cylinders in stationary flow the maximum velocity near the cylinder will be the double of the non-disturbed velocity U_o , see Fig. 4.

In monocromatic waves (potential theory) also the change in velocity will be the double of the non-disturbed acceleration, and the wave force will be the double of the Froude-Krylov force.

$$F = 2 \cdot \rho \cdot \pi \cdot D^2/4 \cdot u = 2 \cdot m \cdot \dot{u} \quad (3)$$

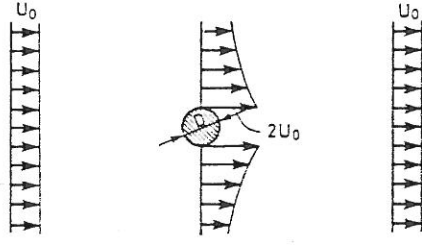


Figure 4: *Flow around circular cylinder according to potential theory.*

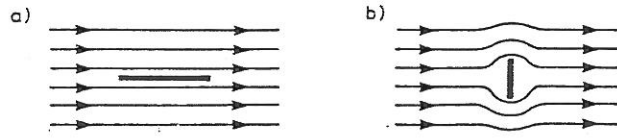


Figure 5: *Streamlines around a flat plate for a) pure skin friction drag, b) pure boundary layer pressure drag (or form drag).*

Introducing the added mass m_a the force can be described as

$$F = (m + m_a) \cdot \dot{u} \quad (4)$$

For other geometries than the circular cylinder the added mass will be different. A sphere has an added mass $m_a = m/2$. This is because the liquid also easily can flow on the upper and under side of the body.

Taking the Froude-Krylov force as basis, the inertia force on a body can be formulated as follows

$$F = C_m \cdot m \cdot \dot{u} \quad \text{where} \quad C_m = 1 + m_a/m \quad (5)$$

No free surface effects were included in the previous considerations.

3 Drag forces

According to the standard definitions the drag force (profile drag force) is regarded as the sum of the skin friction drag, which is the resultant in the drag direction of the shear stress at the surface of the cylinder, and the boundary layer pressure drag (form drag), which results from the pressure distribution in the boundary layer.

Both viscous effects (skin friction drag and form drag) are handled in one, because traditionally it has only been possible to find the forces experimentally without the possibility of separating them. For circular cylinders the form drag will be the very dominant type of the drag force for the relevant range of Reynolds' numbers.

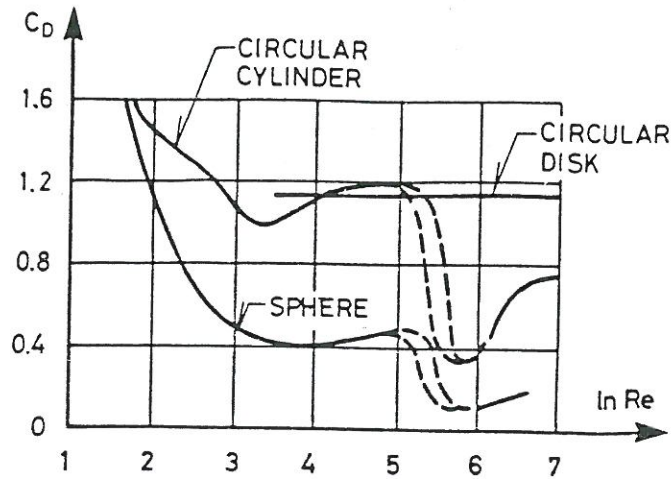


Figure 6: Steady flow drag coefficient for different smooth bodies.

From experiments it is found that the drag force per unit length of the cylinder can be found from the empiric formula:

$$F_D = \rho \cdot \frac{D}{2} \cdot C_D \cdot u \cdot |u| \quad (6)$$

The absolute value of u is introduced in order to synchronize force and flow directions.

For a given shape of the body the drag force must depend on the conditions in the boundary layer, which are given by Reynolds number $Re = (u \cdot D/\nu)$, the relative roughness k and the character (including the turbulence) of the ambient flow. Consequently it is seen that the drag coefficient must depend on Re and k plus the character of the ambient flow field. The last point is significant in oscillatory flow due to reversal of wakes from downstream to upstream side whenever the velocity changes sign.

Fig. 6 shows the steady flow drag coefficients as function of Reynold number for several different smooth bodies ($k/D = 0$). For the circular cylinder and the sphere the drag coefficients change drastically in the region about $Re \simeq 10^5$, where the turbulent vortex trail has developed (compare with fig. 1). This situation corresponds to a transition to turbulent boundary layer where exchange of momentum with the outer flow delays the separation. Consequently the separation points move backwards so the wake behind the cylinder becomes more narrow and the partial vacuum behind the cylinder becomes smaller. This phenomenon is not seen for the disk (flat plate), where the points of separation always will be fixed at the edges of the plate.

In a wave situation the situation is much more complex partly due to the unsteady flow where the velocity vector rotates 360 degrees and partly due to the influence of the history on the instantaneous flow conditions, cf. Fig. 1.

When it comes to practical calculations of the flow force it is important to know whether vortices developed or not before the change in the flow direction. If no vortices are generated the flow will have the character of a potential flow. When, within half a cycle, several vortices have developed the problem can be treated as being quasi-stationary, which means that the flow field in large periods

will be like the stationary flow field. In between the two cases only few vortices are generated and it is much more difficult to predict the flow field. It is mainly for such situations that the Morison equation has found its use.

The best parameter to characterize an oscillatory flow is found to be the Keulegan-Carpenter number $K = U_{max} \cdot T/D$ where U_{max} and T are the velocity amplitude and period of the flow, respectively, and D the diameter of the cylinder.

For small K the potential theory will be valid. For large K the flow will be quasi-stationary. The specific range of K corresponding to the boundaries for the two types of flow are not well defined, mainly because of the dependency on the Reynolds number and the relative roughness which governs the separation of the vortices. In the literature the lower boundary can be found to be $K = 1 - 5$, and the upper boundary $K = 20 - 50$.

Fredsøe 1985 gives the schematic illustration shown in Fig. 7.

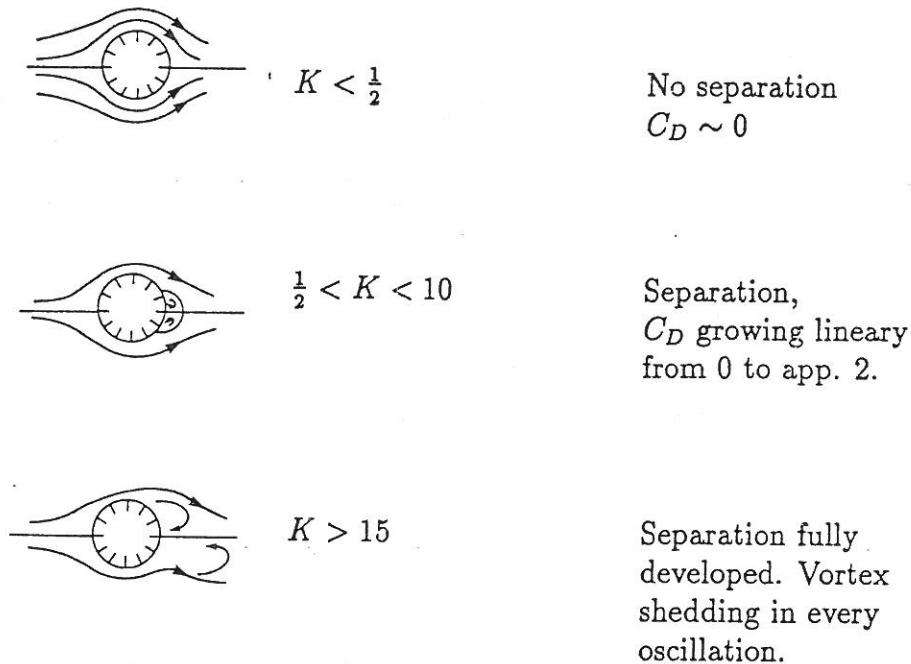


Figure 7: Flow around cylinder depending on K . (Fredse, 1985)

4 Morisons equation for in line forces on cylinders in waves

The Morison equation (1) is purely deterministic, and it is based on a linear combination of the inertia force and the drag force. The formula was published by Morison et al. (1950) as a result of force measurements on piles due to the action of progressive waves.

The inertia term and the drag term in Morison's equation can be perceived to represent the situations where inertia forces or viscous forces dominate.

The inertia forces will dominate when Re is large and K is small, and the drag forces will dominate when Re is small and K is large. Sarpkaya and Isaacson 1981 states that for $K < 10$ the inertia term will be dominating and for $K > 15$ the drag term will be dominating.

The superposition of the drag and inertia components for the general case of wave motion where the flows are unsteady, non-uniform and viscous, may be adopted if it is recognized that the corresponding drag and inertia coefficients no longer retain their values deriving from the two reference flows, but are treated as empirical and taken to depend on the various parameters characterizing the flow.

4.1 Methods for estimation of C_d and C_m

It is obvious that the wave forces are very sensible to the values of C_d and C_m . Moreover, correct application of Morison's equation presume detailed knowledge of the velocity and acceleration field in the oscillatory wave.

The water particle kinematics are often calculated rather than measured and may be determined from wave theories such as linear 1. order, Stokes second or fifth order, cnoidal, solitary etc. For different choices of wave theory the calculated particle kinematics may vary significantly, especially in extreme shallow water.

When using the coefficient in Morison's equation it is very important to be constant and as far as possible use the same wave theory in calculation of the water particle kinematics as was used in the interpretation of the experiments on which the determination of the C_d and C_m coefficients were based.

The determination of C_d and C_m is based on data sets but their meaning depend on the method of evaluation and on the measured force because there is not a unique method of evaluation of a given set of kinematic and dynamic data. Some of the most frequently used methods are as follows:

- a) The least squares technique is based on minimization the square of the difference between the calculated force F_c and the measured force F_m .

For regular waves it means:

$$\int_0^{2\pi} (F_m - F_c)^2 d\theta = \text{minimum} \quad (7)$$

C_d is found from:

$$\frac{\partial \int_0^{2\pi} (F_m - F_c)^2 d\theta}{\partial C_d} = 0 \Rightarrow \quad (8)$$

in case of harmonic waves

$$C_D = -\frac{4}{3\pi} \int_0^{2\pi} \frac{F_m \sin\theta \cdot |\sin\theta|}{\frac{1}{2} \rho U_{max}^2 \cdot D} d\theta \quad (9)$$

C_m is similarly found from:

$$\frac{\partial \int_0^{2\pi} (F_m - F_c)^2 d\theta}{\partial C_m} = 0 \Rightarrow \quad (10)$$

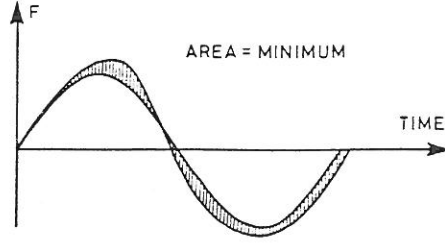


Figure 8: Illustration of the principle in Fourier averaging technique.

$$C_m = -\frac{K}{\pi^3} \frac{\int_0^{2\pi} F_m \cdot \cos\theta d\theta}{\frac{1}{2} \rho U_{max}^2 \cdot D} \quad (11)$$

- b) The Fourier averaging technique is based on a minimization of the area between the calculated force F_c and the measured force F_m .

In case of a harmonic wave the Morison equation can be written as

$$F = \frac{1}{2} \rho \cdot D \cdot U_{max}^2 \cdot \left(C_D \cdot \sin\theta \cdot |\sin\theta| - C_m \cdot \frac{\pi^2}{K} \cdot \cos\theta \right) \quad (12)$$

By multiplying (12) with $\sin\theta$ and $\cos\theta$ respectively and integrating over one cyclis the coefficients can be found to be

$$C_D = -\frac{\int_0^{2\pi} \frac{F_m}{\frac{1}{2} \rho U_{max}^2 \cdot D} \cdot \sin\theta d\theta}{\int_0^{2\pi} \sin^2\theta |\sin\theta| d\theta} = -\frac{3 \int_0^{2\pi} F_m \sin\theta d\theta}{8 \frac{1}{2} \rho U_{max}^2 \cdot D} \quad (13)$$

$$C_m = -\frac{K}{\pi^3} \frac{\int_0^{2\pi} F_m \cos\theta d\theta}{\frac{1}{2} \rho U_{max}^2 \cdot D} \quad (14)$$

- c) Calculate the C_d and C_m coefficients at the points corresponding to the maximum velocity and acceleration.

The method may give small differences between the measured force and the calculated force in the drag dominated region and in the inertia dominated region. Sarpkaya and Isaacson 1981 states that the method is not recommended in a wide range of K and Re values where both drag and inertia may be of equal importance and highly dependent on the historical effects.

Generally the method describes the time variation of the force badly and the C_d and C_m coefficients are more sensitive to changes in the wave kinematics caused by different interpretation than the other methods.

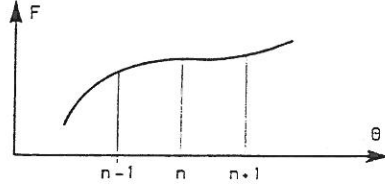


Figure 9: Definition of the times $n - 1$, n , $n + 1$. Tørum 1985)

- d) Time varying C_d and C_m coefficients can be calculated assuming that they are constant within a small time interval $\Delta\theta$ between two force data points. Tørum 1985 gave the following suggestion to determine the C_d and C_m coefficients, Fig. 9.

From the basic equations

$$F_n = \frac{\rho}{2} \cdot D \cdot C_{dn} \cdot U_n \cdot |U_n| + \rho \frac{\pi \cdot D^2}{4} \cdot C_{Mn} \cdot \dot{u}_n \quad (15)$$

$$F_{n+1} = \frac{\rho}{2} \cdot D \cdot C_{dn} \cdot U_{n+1} \cdot |U_{n+1}| + \rho \frac{\pi \cdot D^2}{4} \cdot C_{Mn} \cdot \dot{u}_{n+1} \quad (16)$$

the C_d and C_m coefficients may be found.

$$C_{Dn} = \frac{F_n \cdot \dot{U}_{n+1} - F_{n+1} \cdot \dot{U}_n}{\frac{\rho}{2} \cdot D \cdot (U_n \cdot |U_n| \cdot \dot{U}_{n+1} - U_{n+1} \cdot |U_{n+1}| \cdot \dot{U}_n)} \quad (17)$$

$$C_{M-n} = \frac{F_n \cdot U_n^2 - F_{n+1} \cdot U_{n+1}^2}{\frac{\rho}{2} \cdot \frac{\pi \cdot D^2}{4} (\dot{U}_n \cdot U_{n+1} \cdot |U_{n+1}| - \dot{U}_{n+1} \cdot U_n \cdot |U_{n+1}|)} \quad (18)$$

Fig. 10 shows an example of the method.

- e) Mainly based on figures like Fig. 10. Sarpkaya and Isaacson 1981 and many other authors have concluded that the large variations in $C_d(\theta)$ and $C_m(\theta)$ necessitate an extension of the Morison equation.

Originally this idea was proposed by Keulegan and Carpenter, who expressed the force in terms of a Fourier series assuming the force to be an odd-harmonic function:

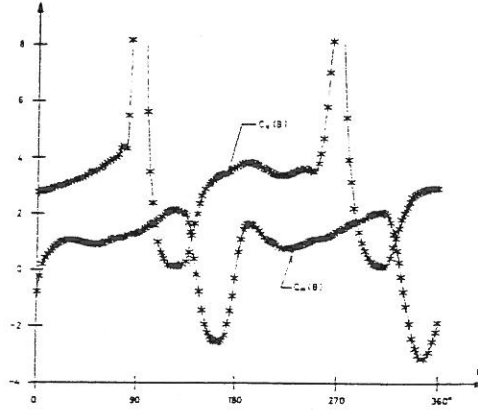


Figure 10: Time varying C_d and C_m coefficient. $K = 12$, $Re = 12540$. From Sarpkaya and Isaacson 1981.

$$\frac{F}{\frac{1}{2}\rho \cdot D \cdot U_{max}^2} = 2[A_1 \sin \theta + A_3 \sin 3\theta + A_5 \sin 5\theta + \dots + B_1 \cos \theta + B_3 \cos 3\theta + B_5 \cos 5\theta + \dots] \quad (19)$$

Following the Morison equation the formula (19) can be rewritten:

$$\frac{F}{\frac{1}{2}\rho \cdot D \cdot U_{max}^2} = \frac{\pi^2}{K} C_m \cdot \sin \theta + 2[A_3 \sin 3\theta + A_5 \sin 5\theta + \dots] - C_d \cdot |\cos \theta| \cdot \cos \theta + 2[B_3 \cos 3\theta + B_5 \cos 5\theta + \dots] \quad (20)$$

1986 Dummer et al. extended the Morison equation to:

$$\begin{aligned} \frac{F}{\frac{1}{2}\rho \cdot D \cdot U_{max}^2} = & \frac{\pi^2}{K} \cdot C_m \cdot \sin \theta - C_D \cdot |\cos \theta| \cdot \cos \theta + \\ & \Lambda^{-\frac{1}{2}} \cdot (0.01 + 0.1 e^{-0.08(K-12.5)^2}) \cdot \\ & \cos [3\theta + \Lambda^{-\frac{1}{2}} (0.05 + 0.35 e^{-0.04(K-12.5)^2})] + \\ & \Lambda^{-\frac{1}{2}} [0.0025 + 0.053 e^{-0.06(K-12.5)^2}] \cdot \\ & [5\theta - \Lambda^{-\frac{1}{2}} (0.25 + 0.60 e^{-0.02(K-12.5)^2})] \end{aligned} \quad (21)$$

Λ being $(2 - C_m)/K \cdot C_D$.

Sarpkaya and Isaacson 1981 investigated the difference between the measured and the calculated force in term of the residue.

Sarpkaya and Isaacson 1981 gave the following suggestion to the force coefficients. The included third term depends on C_m and the K

$$\frac{F}{\frac{1}{2}\rho \cdot D \cdot U_{max}^2} = \frac{\pi^2}{K} C_m \cdot \sin \theta - C_D |\cos \theta| \cos \theta + \longrightarrow$$

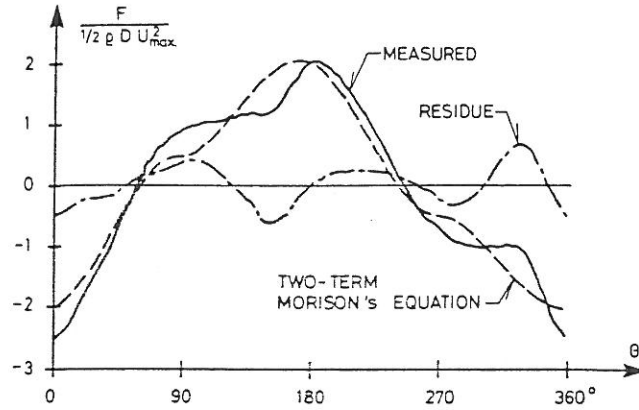


Figure 11: Comparison of the measured force with that calculated from the two-term Morison equation, $K = 14$ and $Re = 27800$. (Sarpkaya and Isaacson 1981).

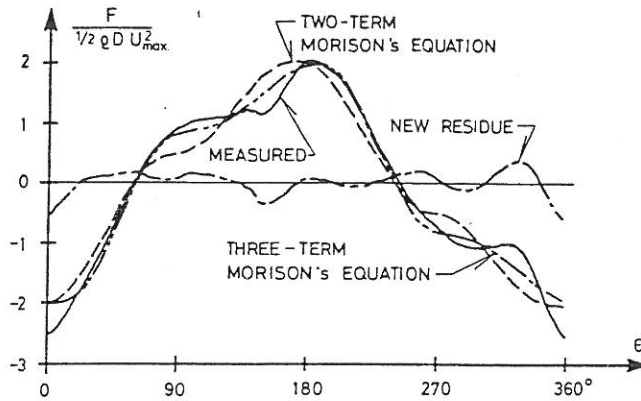


Figure 12: Comparison of the measured force and the calculated force respectively using the two term and the three term Morison equation. $N = 14$, $Re = 27800$. (Sarpkaya and Isaacson 1981).

$$\left(\frac{Re}{K}\right)^{3/4} \cdot \left[\frac{2 - C_m}{100 K} \cdot \cos \left(3\theta + \frac{(K - 4)(2 \cdot C_m)}{2 K} \cdot \pi \right) \right] \quad (22)$$

The three term Morison equation proposed by Sarpkaya and Isaacson and the four term Morison equation proposed by Dummer et al. 1986 have the large advantage that it in contradiction to proposals from other authors does not introduce extra independent coefficients in the equation.

No matter in which way the C_d and C_m coefficients are fitted the problem is: How are the K number and the Reynolds number defined. This may especially be a problem when the time varying coefficients are used, or when irregular waves are treated.

For time varying C_d and C_m coefficients it is usual to use the standard definition for the Keulegan-Carpenter number $K = U_{max} \cdot T/D$ and $Re = \frac{D \cdot U_{max}}{\nu}$. Coefficients based on measurements in irregular waves the U_{max} and T could be

respectively the velocity amplitude and the period for the significant wave.

4.2 Influence of the Keulegan-Carpenter number and the Reynolds number on C_d and C_m in oscillatory flow

Physical considerations and simple dimensional analysis show that C_d and C_m are time-dependent and functions of Keulegan-Carpenter number K , the Reynolds number Re and the relative roughness k/D .

No matter the discussion of the C_d and C_m coefficients together with the basic Morison equation, the following will be based on correctness of this formula.

In this section a review of the Keulegan-Carpenter number and the Reynolds numbers effect on the drag and inertia coefficients will be given. Most of the conclusions are taken from Sarpkaya and Isaacson 1981, who made an excellent analysis based on Keulegan-Carpenter's experiments from 1958 and Sarpkaya's experiments from 1976.

All experiments reported in this section were performed with smooth cylinders in oscillatory flow generated in a U-tube, and C_d and C_m were determined as the Fourier averaged coefficients, i.e. C_d and C_m are time-invariant.

In the following figures Sarpkaya has introduced the dimensionless frequency parameter β , being the ratio between the Reynolds number and the Keulegan-Carpenter number

$$\beta = \frac{Re}{K} = \frac{D^2}{\nu T} \quad (23)$$

By replacing Re by β one has that C_d and C_m are functions of K , β and k/D .

In comparing Figs. 13 and 15 it is seen that C_m 's dependence on $\beta(Re)$ indicates opposite trends for larger K . It is believed that the data by Sarpkaya shown in Fig. 15 are the more reliable.

Fig. 13-16 show that C_d depends on both K and Re , and decreases with increasing Re for a given K . Furthermore it is seen that C_d for small Reynolds numbers have a maximum at $K \sim 10 - 15$.

At Reynolds number approximately equal to $0.2 - 0.4 \cdot 10^4$, the drag coefficient decreases dramatically and reaches a value of about 0.5 for $Re \simeq 2 - 3 \cdot 10^5$. This is due to the change in the flow characteristics where a turbulent boundary layer is created resulting in the vortex trail to become more narrow. This phenomenon is named the drag crisis. The drag crisis in oscillatory flow depends among other parameters on the frequency of the oscillation. From Fig. 16 it can also be seen that C_d is not always larger for a oscillatory flow than for a steady flow.

At large Reynolds numbers (just after the drag crisis), the drag coefficient reaches a constant value of about 0.65.

Fig. 15. shows that C_d for various constant values of the frequency parameter β decreases with increasing Keulegan-Carpenter number when $K \geq 7 - 14$. For constant Keulegan-Carpenter number C_d decreases when Re increases.

C_m has the value found from potential theory ($C_m = 2.0$) until the Keulegan-Carpenter number range where symmetric vortices no longer exist, $K \simeq 5$. After the minimum at a Keulegan-Carpenter number of app. 12-15 (this is when the transversal vortices normal to the ambient flow are not generated any longer) the

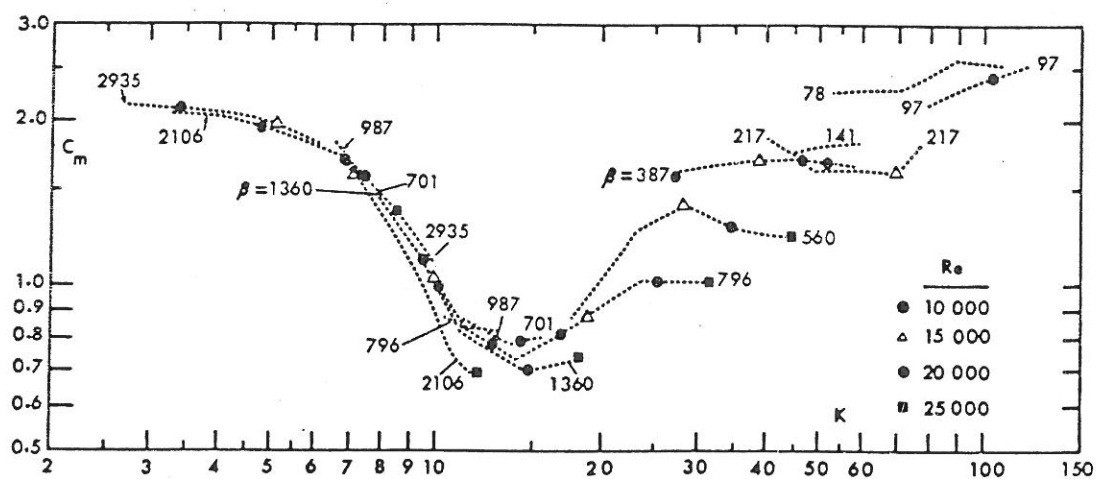
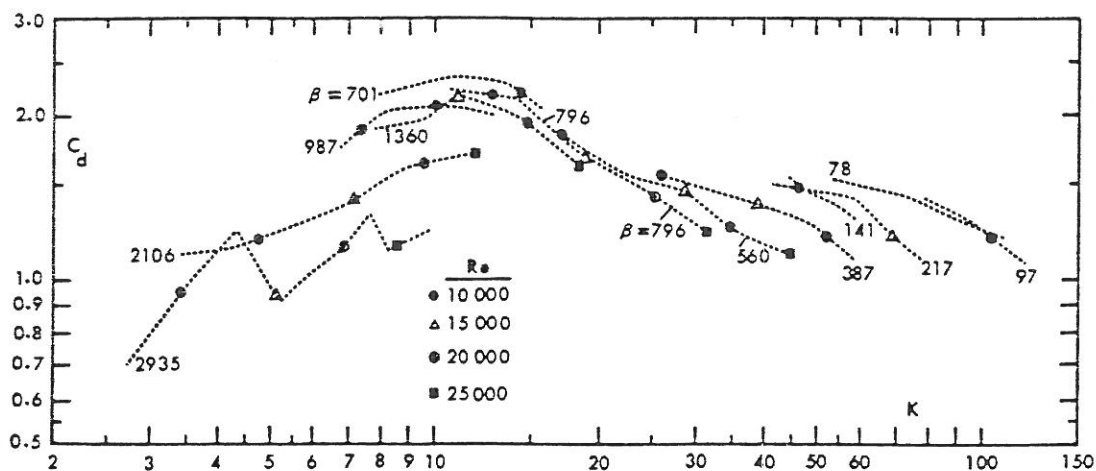


Figure 13: Replot of C_d and C_m from the Keulegan-Carpenter experiments as function of K and the frequency parameter β . Also shown are points representing four selected Reynolds numbers. (Sarpkaya 1976).

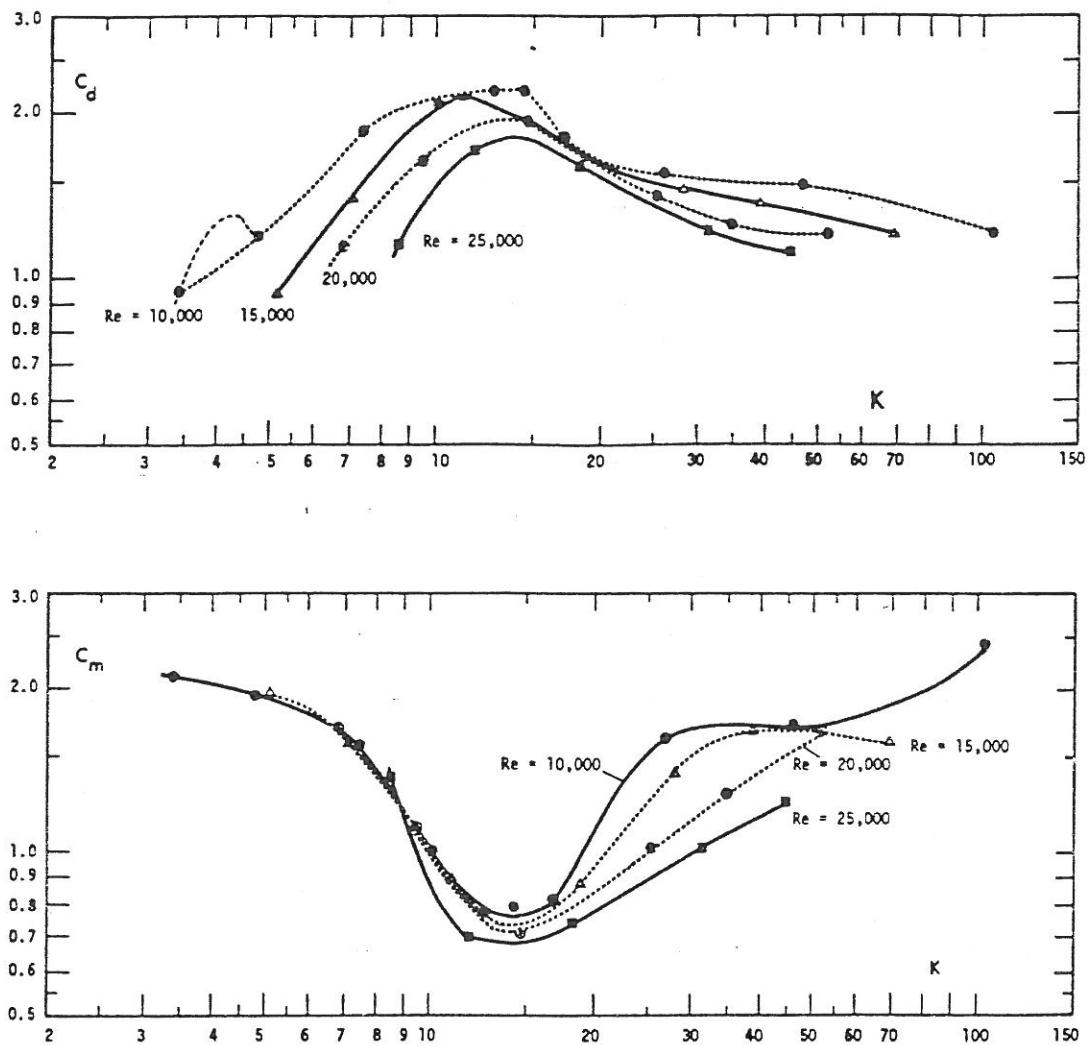


Figure 14: Replot of C_d and C_m from the Keulegan-Carpenter experiments as function of K and Reynolds number. The shown points may be found in Figure 13. (Sarpkaya 1976).

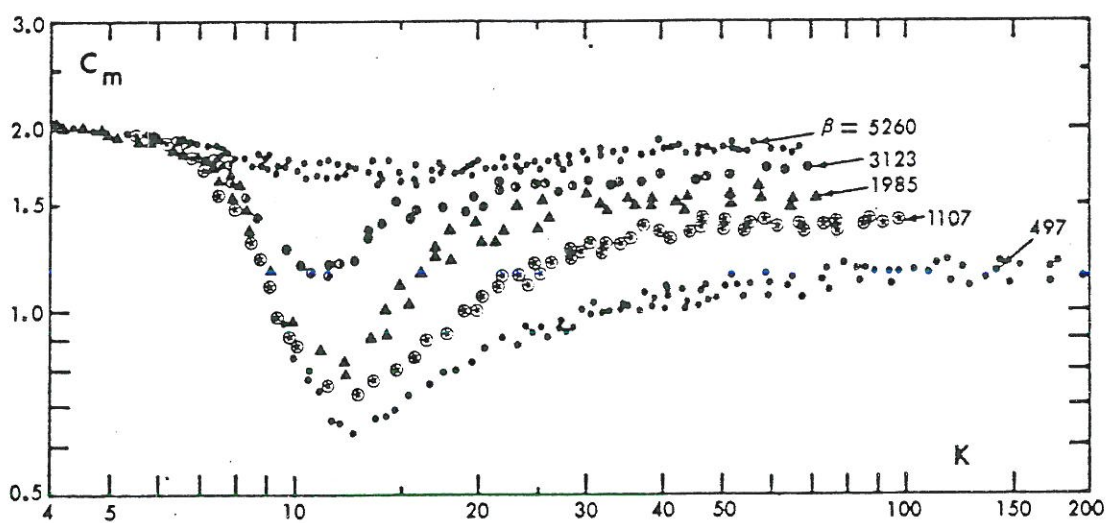
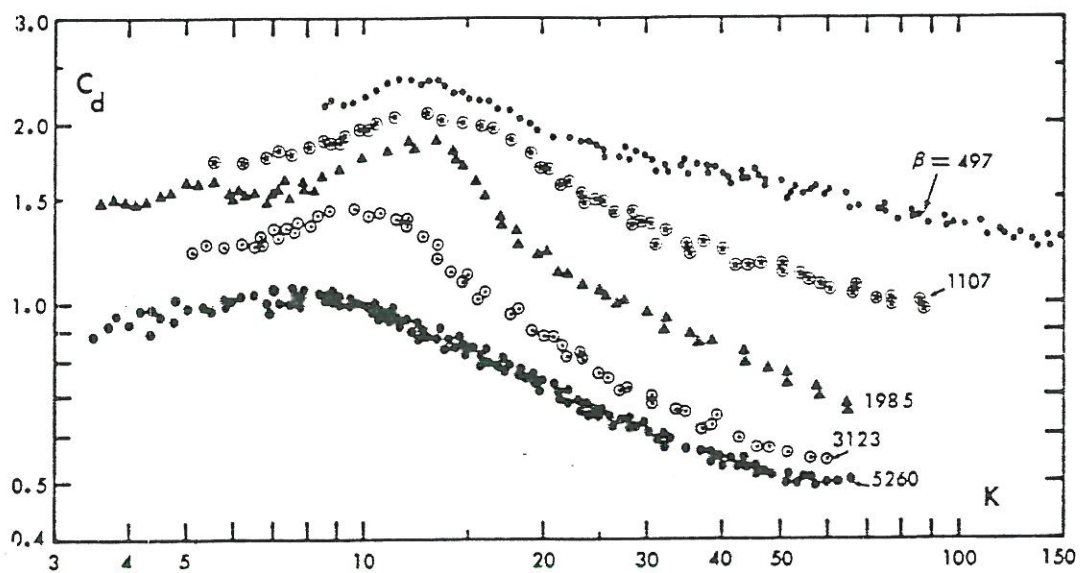


Figure 15: *continued on next page.*

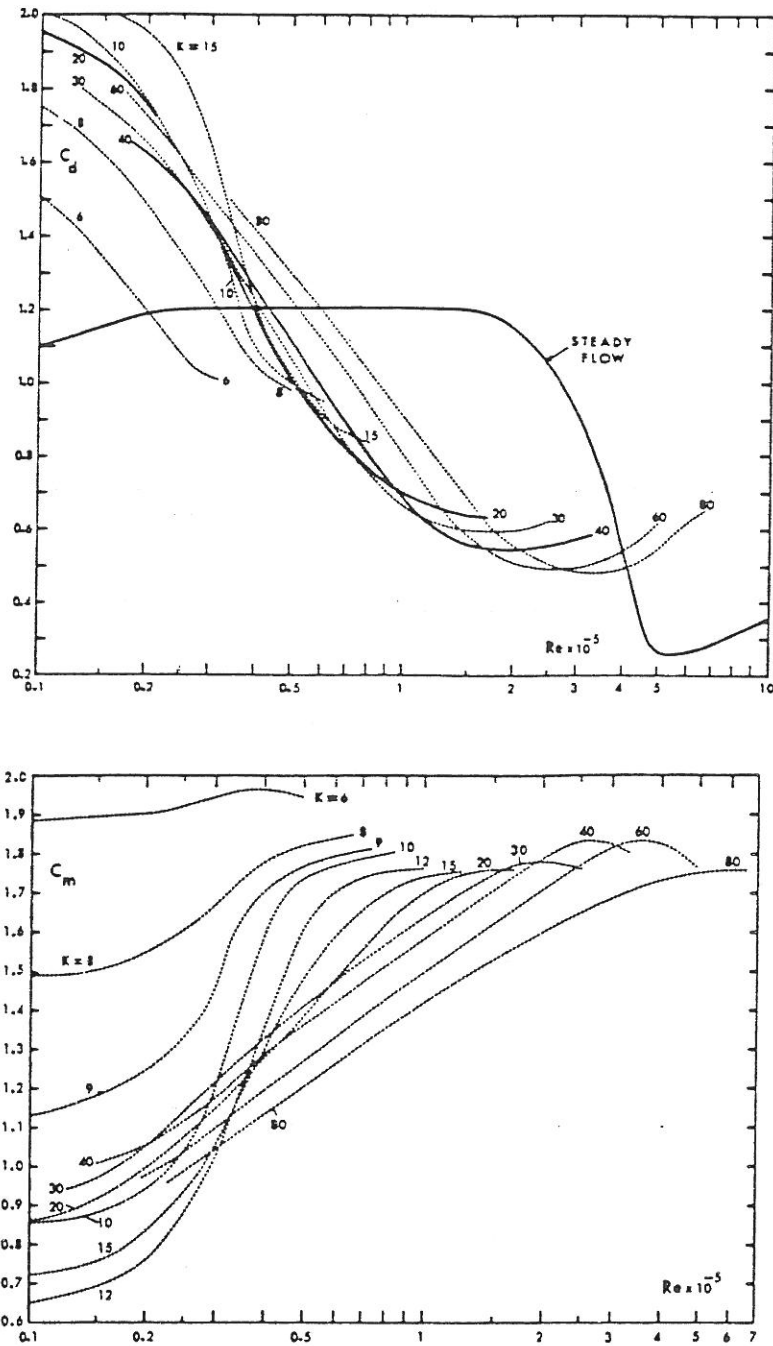


Figure 16: C_d and C_m versus Reynolds number for various values of K . (Sarpkaya 1976).

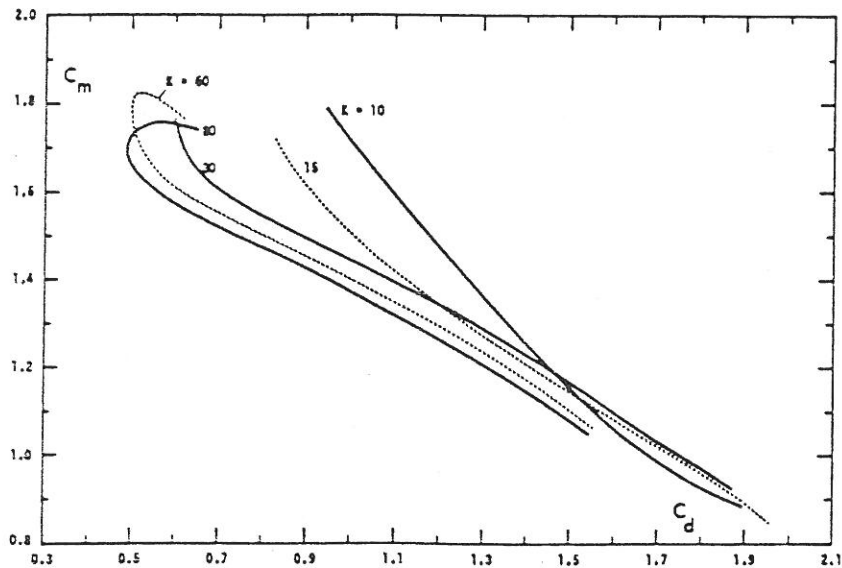


Figure 17: C_m versus C_d for various values of K . The correlation is approximately -1. (Sarpkaya 1976).

inertia coefficient increases with increasing K , until C_m reaches a constant value of 1.8 for large Reynolds numbers.

Generally it can be noted that for large values of the Reynolds number the coefficients seem to be almost constant.

Furthermore, the correlation between the inertia and the drag coefficients are almost -1. This might explain why the Morison equation seems to give reasonable result also in the K and Re range where C_d and C_m change a lot because in this range drag and inertia forces have the same number of magnitude.

4.3 Roughness effect on C_d and C_m in oscillatory flow

Experiments with smooth and sand-roughened cylinders in a U-shaped vertical tunnel were performed by Sarpkaya in 1976. In U-shaped tunnel experiments it is possible to obtain much larger Reynolds numbers than in laboratory generated waves and in addition the flow is uniform along the cylinder. The following Figs. 18-21 from the Sarpkaya experiments show the influence of the relative roughness on the Fourier averages of C_d and C_m .

Adding roughness to a smooth cylinder causes the separation of vortices and the transition to turbulent boundary layer to start at lower Reynolds numbers. The drag crises therefore develops at lower Reynolds numbers the more rough the cylinder is.

It is important to notice that for large Re the change from a smooth cylinder to a cylinder with even a small relative roughness creates many more changes in C_d and C_m than the change from a small relative roughness to a large relative roughness. A change in the drag coefficient of 100% can easily be found for a

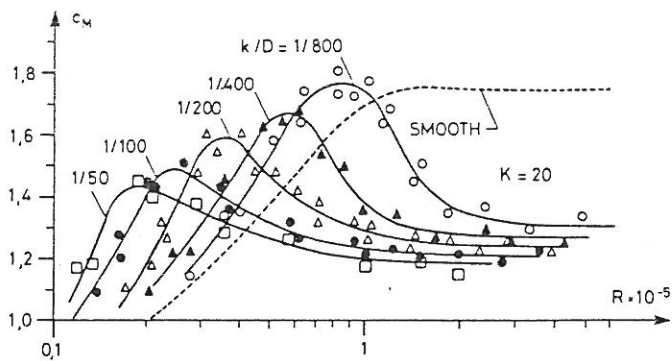
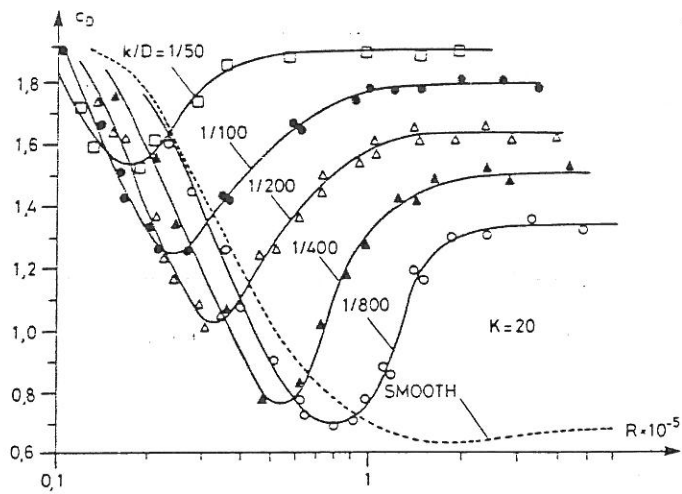


Figure 18: C_d and C_m versus Reynolds number and relative roughness. $K = 20$. (Sarpkaya 1977)

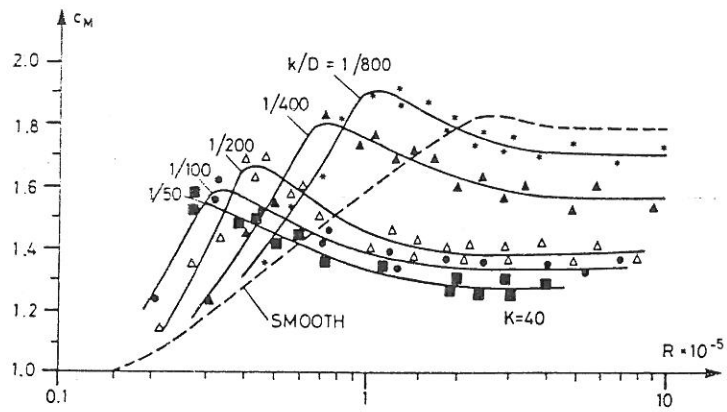
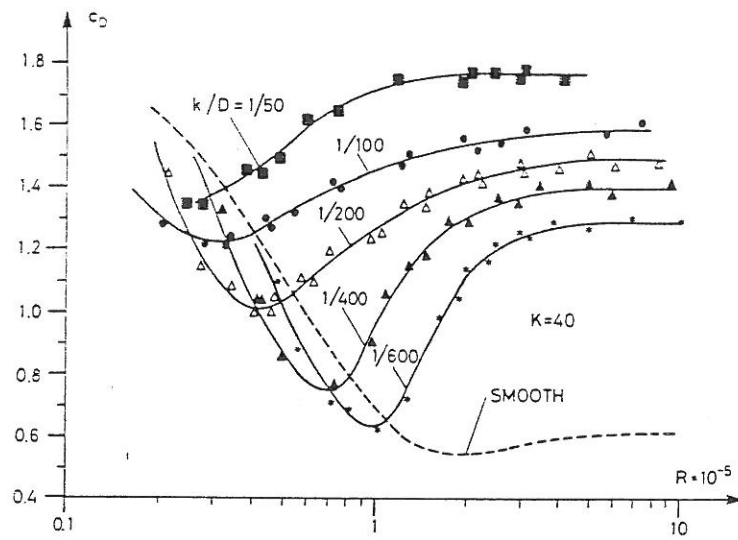


Figure 19: C_d and C_m versus Reynolds number and relative roughness. $K = 40$. (Sarpkaya 1977)

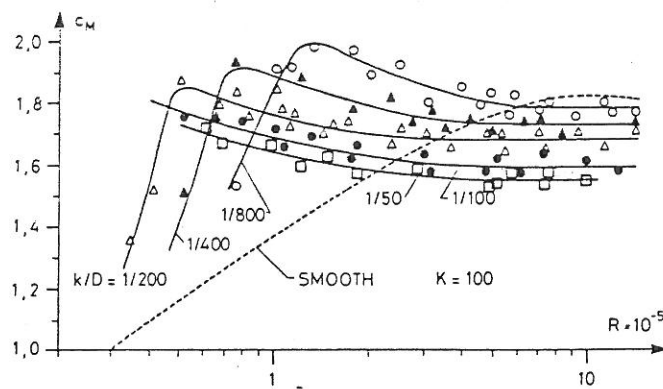
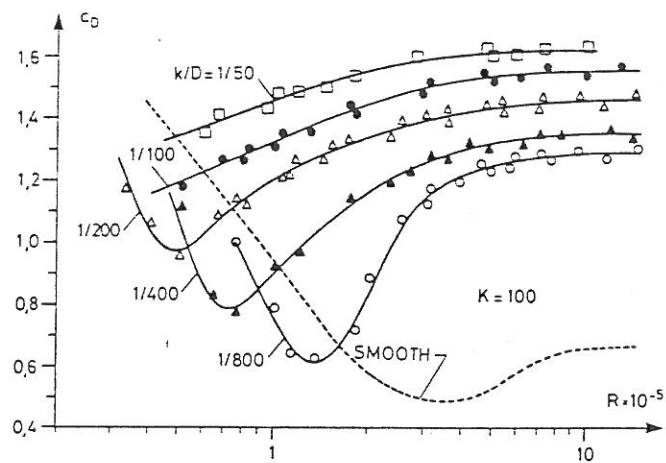


Figure 20: C_d and C_m versus Reynolds number and relative roughness. $K = 100$. (Sarpkaya 1977)

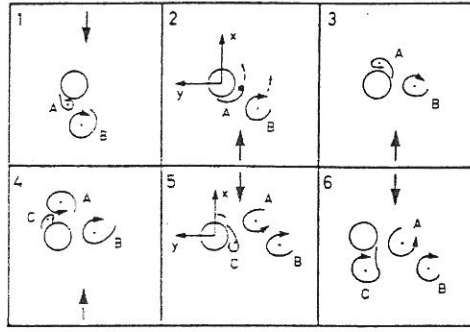


Figure 21: Flow characteristic for $7 < K < 13$. Vortex street normal to the ambient flow. (Williamson 1968)

relative roughness equal to $1/800$. For the inertia coefficient the change is smaller; maybe 10-20%, for a relative roughness equal to $1/800$.

The changes of the C_d and C_m coefficients due to roughness of the cylinder is found to be negatively correlated. This counter-variation is a consequence of the use of Morison's equation with time-invariant coefficients rather than a consequence of a fluid mechanical phenomenon.

4.4 Influence of current on C_d and C_m in oscillatory flow

Normally the influence of current is taken into account by adding vectorally the water particle velocities due to oscillations and current. Morison's equation then becomes

$$F = \frac{1}{2} \rho \cdot D \cdot C_d \cdot (U + U_c) \cdot |U + U_c| + \frac{\pi}{4} \cdot \rho \cdot D^2 \cdot C_m \cdot \dot{U} \quad (24)$$

where U_c represents the velocity of the current. The Keulegan-Carpenter number K and Reynolds number Re may then be calculated as:

$$K = \frac{U_c + U_{max}}{D} \cdot T \quad (25)$$

$$Re = \frac{U_c + U_{max}}{\nu} \cdot D$$

In the drag-inertia dominated regime, the vortices arrange themselves in a vortex street on one side of the cylinder normal to the ambient flow. The side from which the vortices separate may become switched either by the action of random disturbance in the flow or, the restarting of the flow. This flow characteristic is shown in Fig. 21.

In the drag dominated regime a pair of vortices occurs, and a vortex street is created behind the cylinder. For the drag dominated flow the strong transverse pressure gradients are considerably reduced and the double hump in the in-line force

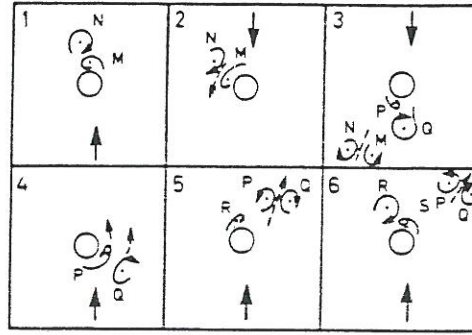


Figure 22: Flow characteristic for $K > 15$. Diagonal vortex street extending from lower left to upper right. (Williamson 1968)

almost disappears, leading to a much better agreement between the measured and the calculated force.

Extensive flow visualization experiments (Sarpkaya and Storm 1985) with oscillating cylinders in uniform flow have shown that the presence of even very small currents have the effect that the transverse half vortex street is very unstable and that the cylinder gets a vortex street behind the cylinder.

Data for C_d and C_m for oscillatory flow with a superimposed steady current are shown in Fig. 23-24. The total velocity has been applied in the analysis, and the resulting force coefficients are slightly smaller than those for pure oscillatory motions. This points to a small relative reduction in the forces compared to the pure oscillation case.

Even though the force coefficients vary very much in the presence of current, Sarpkaya and Storm 1985 found the modified Morison equation as in equation (24) to represent the measured force in a coexisting flow field as well as the original Morison equation in a no-current field.

All the data presented in the previous figures relate to 2-dimensional, rectilinear flow. In real situations with waves, also interactions between wave and current take place.

If the current is in the direction of wave propagation, the wave amplitude decreases and the wave length increases. And when the current opposes the wave, the wave becomes steeper and shorter. These effects make it more difficult to predict the flow field.

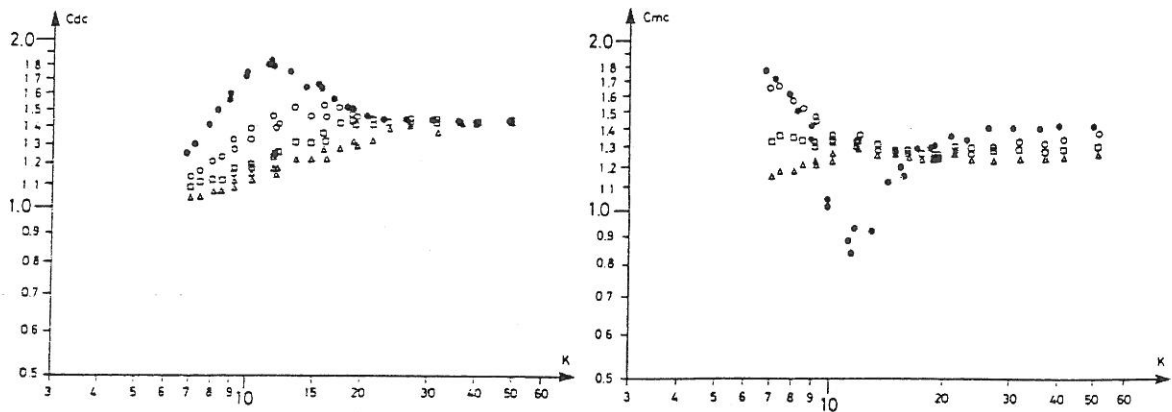


Figure 23: Drag and inertia coefficients versus Keulegan-Carpenter number for cylinder with relative roughness = 1/100 and frequency parameter $\beta = 1800$. (Sarpkaya and Storm 1985)

K_c being the Keulegan-Carpenter number for the current $K_c = U_c T/D$.

- $K_c = 0$
- $K_c = 2$
- △ $K_c = 4$
- $K_c = 6$

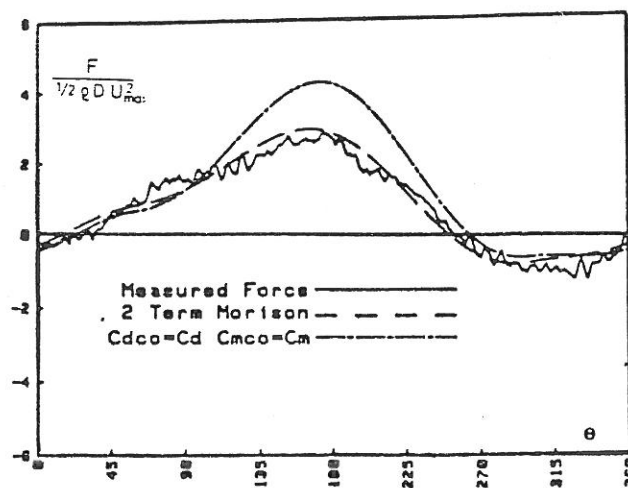


Figure 24: Comparison of measured and calculated forces for a cylinder with relative roughness = 1/100. $\beta = 1800$, $K = 12$, $K_c = 6$. (Sarpkaya and Storm 1985)

4.5 Effect of orbital motions and pile orientation on C_d and C_m

In waves the flow field surrounding the cylinder is always three-dimensional. In wave flows, it is not an easy matter to isolate the effect of orbital motion on cylinder resistance in waves, particularly in the range of practical K and Re values. This is because measurements made with waves reflect not only the effect of orbital motion but also the variation of K and Re with depth.

According to the simple 1st order wave theory, the water particles move in elliptic orbits. Tests at low Reynolds numbers simulating this flow condition have been carried out, cf. Fig. 25 which shows C_d and C_m for a vertical cylinder. The horizontal flow components normal to the cylinder have been used for the calculation of the coefficients. It is seen that C_d decreases and C_m increases in orbital flow compared with the oscillatory flow.

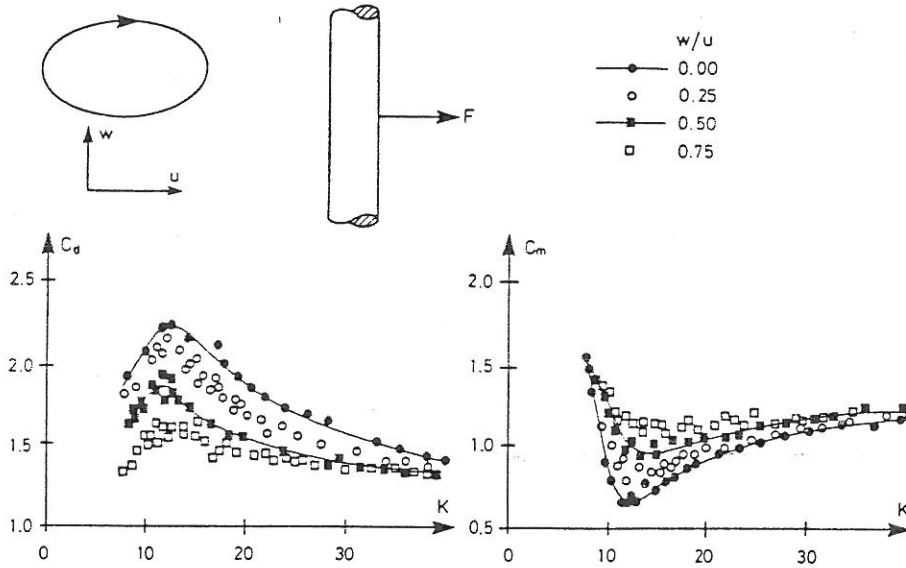


Figure 25: Force coefficients for orbital flow around a vertical cylinder. $K = \frac{|U_{max}| \cdot T}{D}$. (Sarpkaya 1983) $\beta = 784$

The relative larger the vertical flow component the more discrepancy from the oscillatory flow coefficients is seen. This is true especially in the range of importance of both drag and inertia forces $7 < K < 15$ where the flow is complex in beforehand. However, because the variations in C_d and C_m are negatively correlated, the changes in the force are more moderate. Moreover, it turns out that the horizontal flow components (i.e. perpendicular to the cylinder) can be used with good accuracy in the force calculation).

In case of inclined cylinders it is possible to resolve the fluid velocity and acceleration components into net flow vectors which act at an angle α to the cylinder

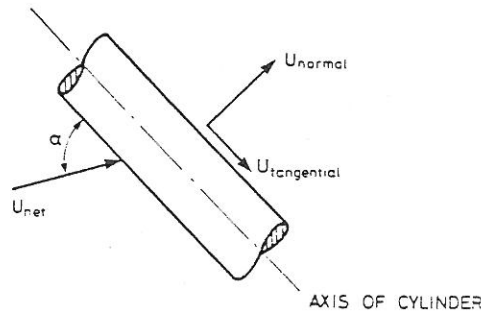


Figure 26: *Decomposition of velocity vector for an inclined cylinder.*

axis. Then one may decompose the vectors into normal and tangential components, and then ignore the tangential components in the calculation of the force.

The decomposition of the velocity vector is shown in Fig 26. The Reynolds number and the Keulegan-Carpenter number should be defined as

$$Re = \frac{|U_n| \cdot D}{\nu} \quad , \quad K = \frac{|U_n| \cdot T}{D} \quad (26)$$

Using $U_{normal} = U_{net} \cdot \sin \alpha$ to evaluate the drag force, one may see that the 'in-line' force is no longer necessarily in-line. Furthermore, the net acceleration and the inertia force may have other directions than the net velocity vector. The total force is found by adding vectorally the drag and the inertia force.

These effects complicate the force calculation further because the lift force (shortly described in chapter 5.0) cannot be separated from the in-line force.

Cotter and Chakrabarti 1984 investigated the force coefficients for inclined cylinders. Water particle velocity and accelerations were calculated using the Stream function theory derived by Dean 1965. Normal velocities and accelerations rather than the horizontal velocities and accelerations were used to determine C_d and C_m by a least square technique. Fig. 28 shows the results of the experiments which covered a Reynold number range of 2000-91000. No influence on the force coefficients were found, but Cotter and Chakrabarti stated that for larger Reynold numbers an effect may be seen.

Fig. 28 indicates that the procedure of using normal components of the particle kinematics is rather good as it produces consistent coefficients, but effects from tangential velocities can still be seen as was the case in the experiments with orbital flow, Fig. 25.

Despite the many investigations already performed, considerable additional work is required in order to obtain a better understanding of the wave forces on oblique members. Until then the use of the principle of normal-component particle kinematics together with drag and inertia coefficients applicable to vertical cylinders is generally recommended.

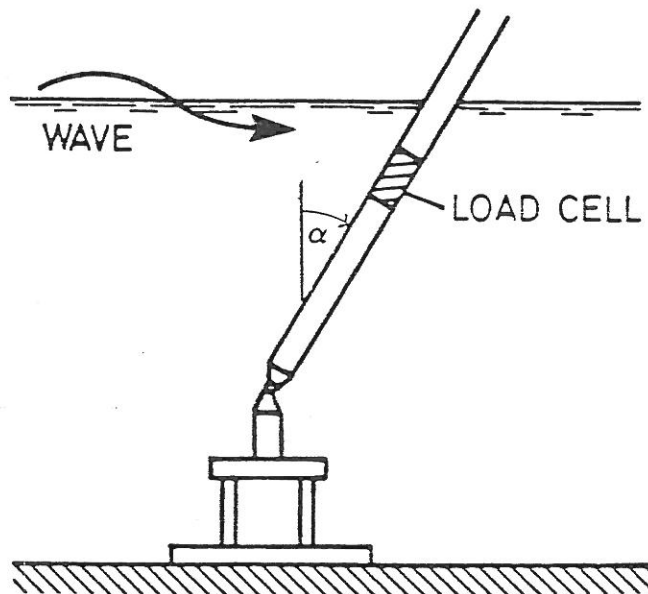


Figure 27: Test setup for inclined cylinder. (Cotter and Chakrabarti 1984)

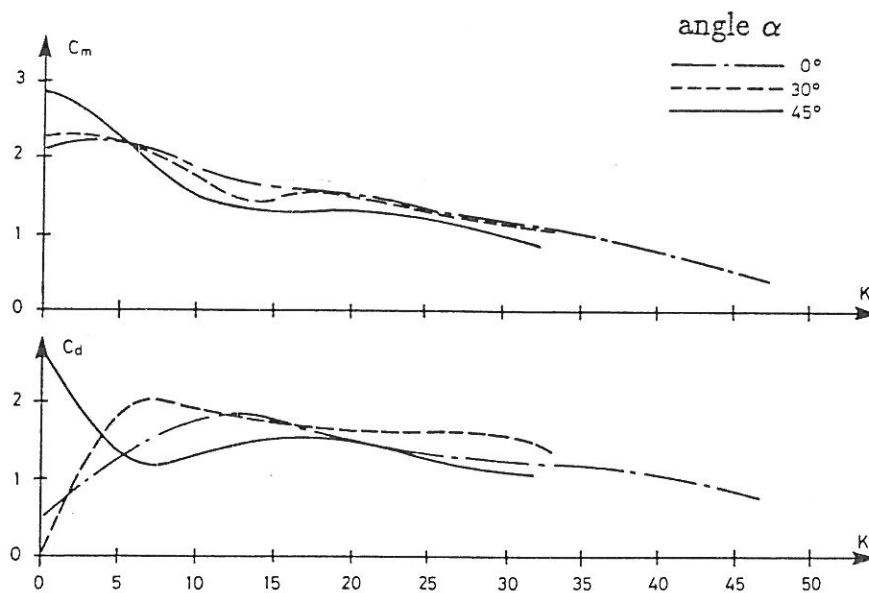


Figure 28: C_d and C_m versus K for a cylinder at 0° , 30° and 45° . Replot from Cotter and Chakrabarti 1984.

4.6 Surface effects on C_d and C_m

The forces in the surface zone usually have considerable influence on the mud-line bending moment. the Morison equation does not predict the force in this zone very well. Fig 29 shows a comparison between measured and calculated force for a very steep but non-breaking wave and for a less steep wave. Time invariants C_d and C_m were used.

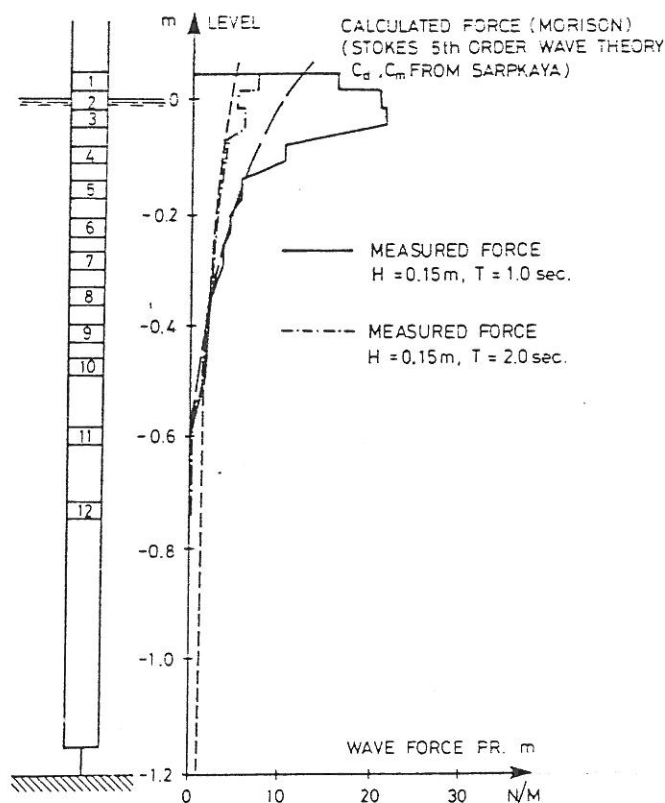


Figure 29: Comparison of measured and calculated force distribution on a smooth cylinder. (Frigaard 1988). $C_d = 1.0$ $C_m = 1.8$. Waterdepth = 1.2 m.

At the time of maximum force the maximum contribution the major contribution to the force in the surface zone may be assumed drag. On the upstream side there is a run-up equal to the pressure head, on the downstream side there is a transitional zone from the zero pressure at the maximum draw down point to the point where the quasi-hydrostatic pressure is equal to the negative pressure behind the cylinder as indicated on Fig. 30, where also the force intensity is indicated.

Dean et al. 1981 analysed the wave and force data from the Wave Projects I and II. A comparison between measured forces and calculated forces using stream function theory to predict the wave kinematics were performed. In Fig 30 the ratio of the predicted force F_p to the measured force F_m were plotted against the

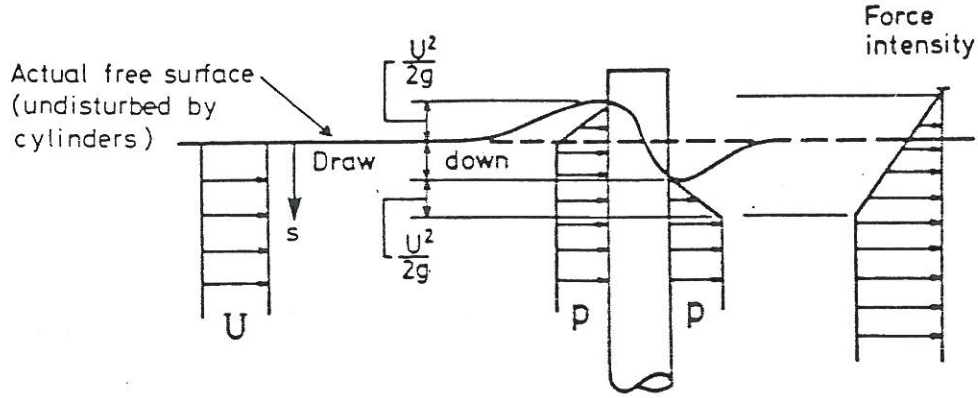


Figure 30: Sketch of surface force intensity along cylinder exposed to waves. (Tørum 1985)

dimensionless submerged distance

$$s' = -\frac{s}{U^2/2g} \quad (27)$$

where s is defined in the figure.

To develop an empirical relationship, the data were sorted according to increment 0.25 of s' . The average values of predicted in-line forces were calculated, but only for waves with Reynolds numbers larger than $2 \cdot 10^6$. To develop an empirical relationship the ratio F_p/F_m were plotted against s' for dynamometers at two different levels. Both dynamometer levels resulted in approximately the same form of the ratio, which were fitted to be

$$\frac{F_p}{F_m} = 1 + e^{-0.188 s'^2} \cdot \cos 0.925 s' \quad (28)$$

Based on the empirical fit (27) the effect of the free surface on the force distribution was included in Morisons equation as follows

$$F = V \cdot C_D \cdot \frac{\rho}{2} \cdot |U| \cdot U + C_m \cdot \frac{\rho \cdot \pi \cdot D^2}{4} \cdot \dot{U} \quad (29)$$

in which

$$V^{-1} = \begin{cases} 1.0 + e^{-0.188 s'} \cdot \cos 0.925 \cdot s' & s' \leq -1 \\ -1.37 + \frac{6.37}{(1-s')^{1.15}} & -1 \leq s' < 1 \end{cases}$$

Tørum 1985 recommended the use of modified force coefficient based on C_d and C_m values found without free surface modifications, Fig. 32. The force coefficients should be used together with kinematics calculated using the 2nd order wave theory.

It should be noted that impacts from breaking waves can cause surface effects considerably different from the ones presented here.

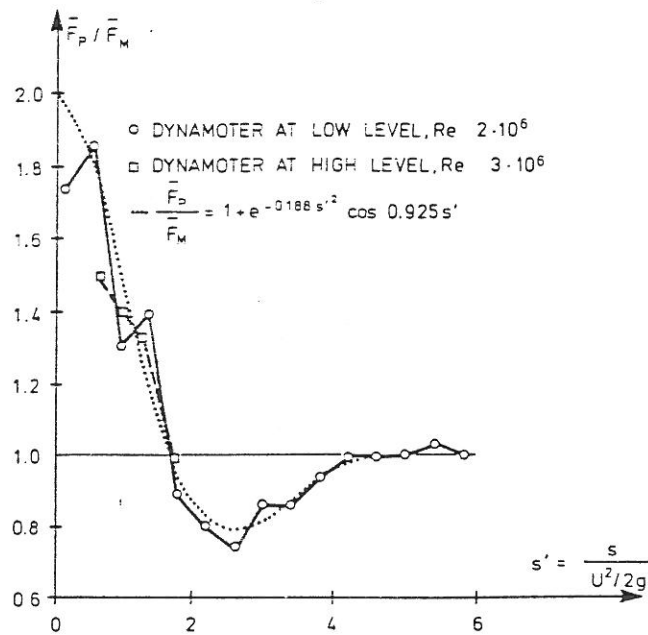


Figure 31: Free surface effect as shown by the ratio of predicted to measured forces as a function of free-surface proximity. (Dean et al. 1981)

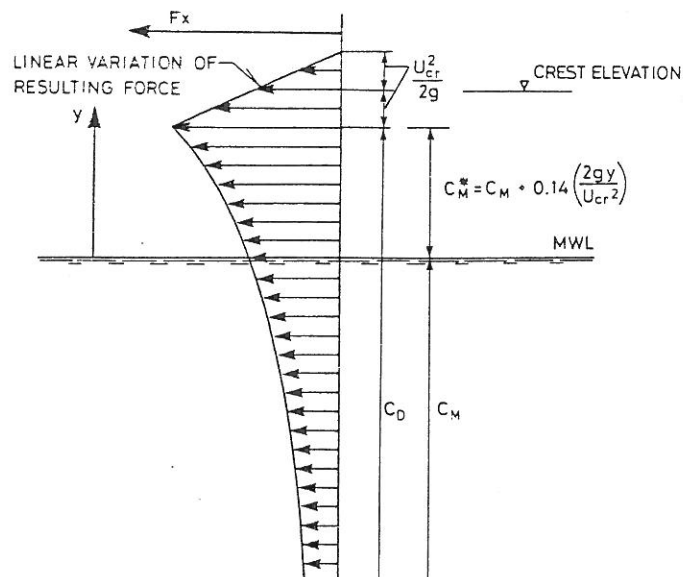


Figure 32: Recommended time invariant force coefficients in the surface zone area. (Tørum 1985).

4.7 Group effects (interference)

So far only C_d and C_m coefficients for a single cylinder have been treated. Because many marine structures are multimember structures, it is important to know if any interference takes place.

The interference effect is depending on parameters like pile spacing, wave direction, roughness and turbulence of the flow.

The wake of an upstream cylinder can have a profound effect on the fluid forces on a downstream cylinder. The wake contains turbulence which can trigger a reduction in the drag force, due to a drag crisis at smaller Reynolds numbers than expected.

An example of the effect of a neighbour cylinder on the drag of an inline placed test cylinder as function of the cylinder spacing is shown in Fig. 33 taken from Laird et al. 1971. Both uniform and oscillatory flow are presented. Whereas the neighbour cylinder influences the drag on the shielded test cylinder considerably even for a spacing of 10 diameters, the influence is seen to be zero in case of oscillatory motions for a cylinder spacing of 4 diameters. This indicates that the interference effects are less pronounced in oscillatory flow than in uniform flow. No dependency on the Keulegan-Carpenter number and Reynolds number were reported.

Sarpkaya found that as the amplitude of flow oscillation becomes comparable or smaller than the gap between the two cylinders, the drag and inertia coefficients gradually approach those corresponding to an isolated cylinder.

Sarpkaya also found that very large transverse forces can occur when the line joining the centres of the cylinders is not parallel to the flow direction.

For a more detailed discussion of flow interference see Sarpkaya and Isaacson 1981.

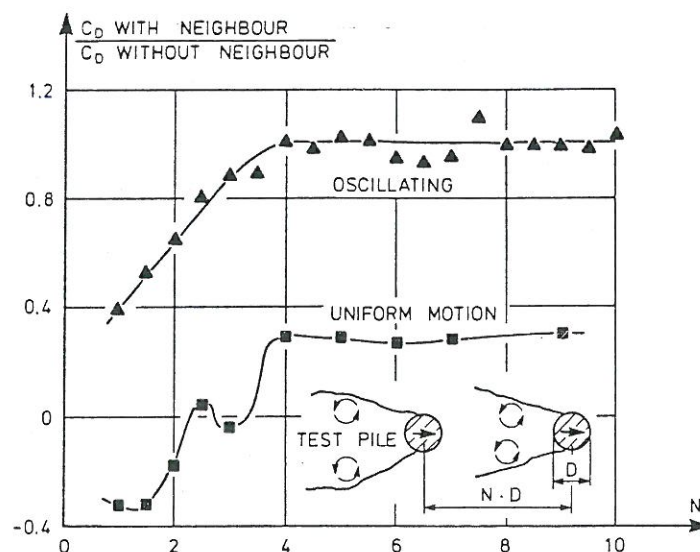


Figure 33: Variation in C_d -ratio versus cylinder spacing. (From Olsen, based on Laird et al. 1971)

5 Transverse forces and spanwise correlation

Morison's equation is only concerned with in-line forces and cannot be used to predict transverse forces induced by the shedding of vortices, see Fig. 2. Any asymmetry that develops around the cylinder will result in a transverse (lift) force, and the variation in time of the lift force will be a complex combination of the effect of the oscillatory flow and the shedding rate of the vortices.

A very simple model for the lift force in oscillatory flow is

$$F_L = \frac{1}{2} \rho \cdot U_{max}^2 \cdot C_l \quad (30)$$

where C_l is denoted the lift coefficient.

The transverse force on a cylinder in oscillatory flow has been investigated by Sarpkaya 1977. The data for the maximum lift coefficient C_l for smooth cylinders are presented in Figs. 34-35, where C_l is defined as maximum amplitude of the transverse force/ $0.5 \cdot \rho \cdot D \cdot U_{max}$. Sarpkaya found that C_l were almost independent of the relative roughness k/D .

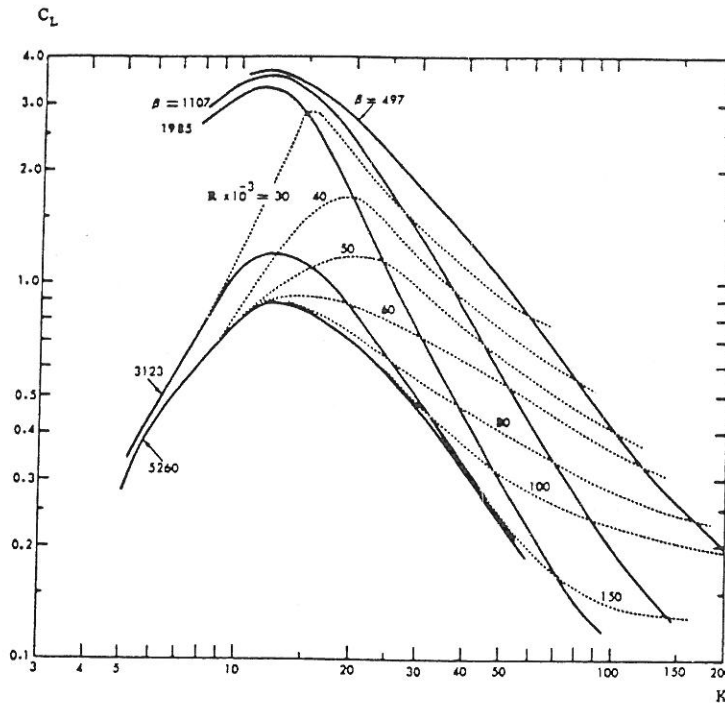


Figure 34: Lift coefficient versus the Keulegan-Carpenter number K for various values of the frequency parameter β and Reynolds number Re . $k/D \sim 0$. (Sarpkaya 1977).

From Fig. 34-35 it is seen that C_l is maximum for a Keulegan-Carpenter number of approximately 13. This is not surprising because in this range of K the asymmetry in the vortex shedding is very pronounced.

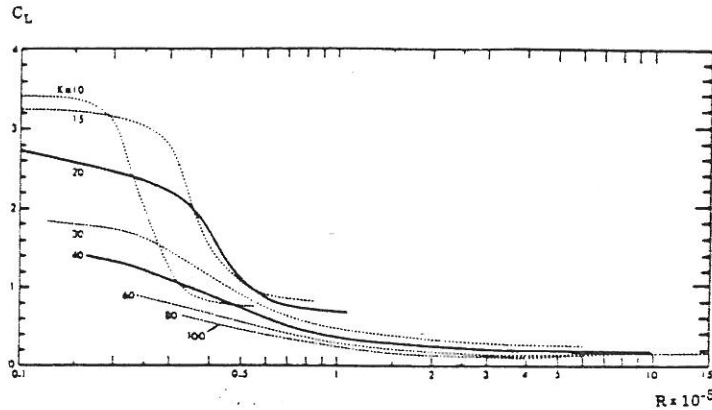


Figure 35: *Lift coefficient versus Reynolds number for various values of the Keulegan-Carpenter number. $k/D \simeq 0$. (Sarpkaya 1977).*

It is evident that the lift force acting on the cylinder is a major portion of the total force acting on the cylinder. Fortunately the maximum lift force is out of phase with the the maximum in-line force. Consequently the maximum in-line force is a fairly good estimate on the maximum total force.

The alternating nature of the transverse force is just as important as its magnitude. The frequency of the transverse force is shown in Fig. 36 in terms of the relative frequency f_r , defined as the frequency of the transverse force divided by the frequency of the oscillatory flow. It is apparent that f_r is not constant and increases with increasing K and Re . Because all vortices are not necessarily fully developed and shed, f_r is not necessarily an integer. This phenomenon is particularly common for f_r values in the neighbourhood of 3 and also for large values of K and Re where the oscillations of the transverse force becomes quite irregular.

It is on the safe side to assume that the three-dimensionality of the flow will reduce the correlation length along the cylinder. The lift coefficients presented in Figs. 34-35 represent the maximum local values.

Tørum and Reed 1982 investigated the spanwise correlation along a slender cylinder by measurement of the transverse force at various fixed levels. Tests performed in regular as well as in irregular waves showed that the transverse force in both cases were irregular.

If the forces at each specific level acted simultaneously in the same direction then for a given probability the summation of forces recorded at different levels should be exactly the same as the distribution of the recorded summerized force. Fig. 37 shows that this is not the case. Consequently there is not full correlation of the transverse forces along the cylinder.

The net effect of the spanwise variations of the vortex tube is that the transverse lift coefficients obtained from a measurement of the total transverse force is not necessarily identical to those calculated from measurements of transverse forces at different levels.

The spanwise correlation of the transverse force along a cylinder might be

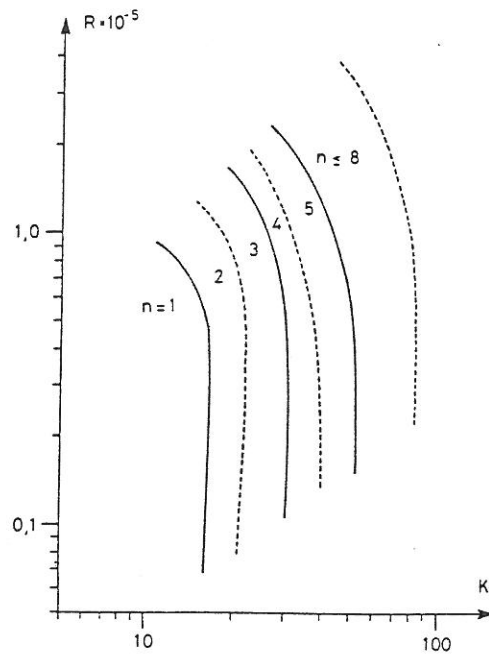


Figure 36: Relative frequency f_r of vortex shedding as function of K and Re for a smooth cylinder. (Sarpkaya 1977).

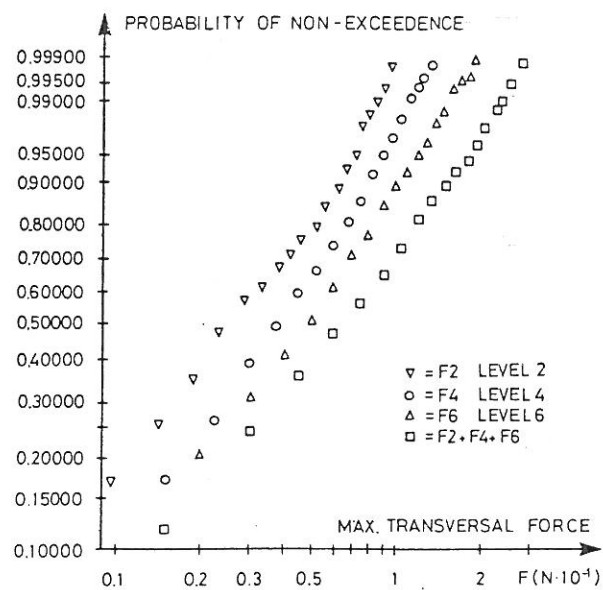


Figure 37: Distribution of force peaks for the individual transversal forces at various levels along a vertical smooth cylinder. (Tørum and Reed 1982).

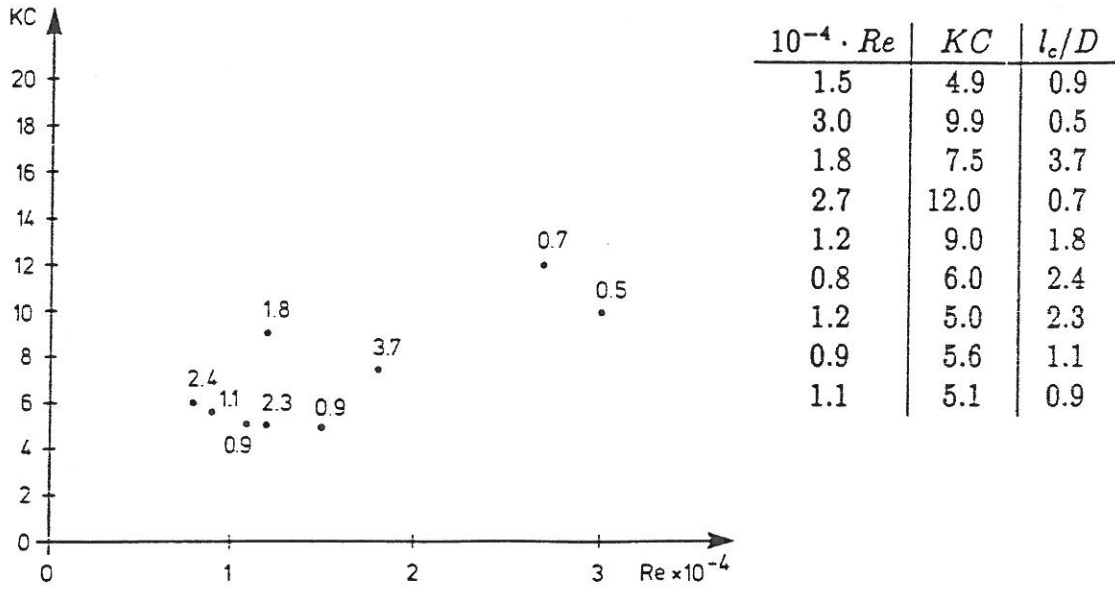


Figure 38: Examples of dimensionless correlation length l_c/D for transverse forces. Experiments with smooth vertical cylinder in regular waves. (Frigaard 1988).

expressed in terms at correlation function or normalized covariance function

$$\rho_{F_y F_y}(z, \Delta z) = E[F_y(z) \cdot F_y(z + \Delta z)] / \sqrt{E[F_y^2(z)] \cdot E[F_y^2(z + \Delta z)]} \quad (31)$$

where z is a coordinate along the cylinder.

The length scale l_c defined by (31) corresponds to the part of the cylinder along which full correlated transversal force should act in order to give same resulting transverse force as the total measured force over $\max \Delta z$

$$l_c(z) = \int_{-\infty}^{\infty} \rho_{F_y F_y}(z, \Delta z) d(\Delta z) \quad (32)$$

Fig. 38 shows an example of $l_c(z)$ corresponding to long crested regular waves (with mean water level as reference point). As seen $l_c(z)$ is not a simple function of K and Re . Furthermore the results reflect only a very narrow Reynold number range. The experiments indicate rather small correlation lengths.

6 Effects of wave directionality

The determination of wave loads on cylinders are generally based on the application of one-dimensional frequency spectra representing long-crested (or 2-dimensional, 2-D) seas. However, natural wind generated waves in the open sea are short crested (or 3-dimensional, 3-D) with directional spread of component waves.

It is to be expected that a 3-D wave representation of a specific surface elevation time series will result in forces which are somewhat lesser than those predicted by 2-D wave representation of the same time series. This might be illustrated by considering a free surface elevation amplitude produced by the crossing of two

regular waves propagating at an angle to each other. The resulting horizontal fluid velocities and accelerations and relating forces on a body are generally smaller than those of a single regular wave with the same free surface amplitude.

The 3-D waves are described by the two-dimensional spectra

$$S(f, \theta) = S(f) \cdot G(f, \theta) \quad (33)$$

where $S(f)$ is the one-dimensional spectra and $G(f, \theta)$ is a directional spreading function.

The one-dimensional frequency spectra may be obtained by integrating the corresponding directional spectra over θ

$$S(f) = \int_{-\pi}^{\pi} S(f, \theta) d\theta \quad (34)$$

It follows that $G(f, \theta)$ must satisfy

$$\int_{-\pi}^{\pi} G(f, \theta) d\theta = 1 \quad (35)$$

Various semi-empirical expressions for $G(f, \theta)$ have been proposed. In many cases G is considered independent of frequency and given as a cosine-power function, i.e.

$$G(\theta) = C(s) \cos^{2s} \left[\frac{1}{2}(\theta - \theta_0) \right] \quad (36)$$

where $C(s)$ is a normalizing function needed to ensure the identity (34) and θ_0 is the direction about which the spectrum is centered. The normalizing function is given by

$$C(s) = \frac{1}{2\sqrt{\pi}} \frac{\Gamma(s+1)}{\Gamma(s+\frac{1}{2})} \quad (37)$$

where Γ is the Gamma function. s describes the degree of spread about θ_0 . Small values of s correspond to a wider spread.

In 1976 Hydraulic Research Station, Wallingford found that in seas with $\cos^2\theta$ continuous distributions of energy between $\pm\pi/2$ the in-line forces on a vertical cylinder were 87% of the in-line force in a long crested sea with the same total energy. The transverse forces in the short crested sea were found to be 50% of the in-line forces in the long crested sea.

The experiments at Wallingford were performed with fairly large cylinders and the results can not be employed directly to slender cylinders. Nevertheless, the reduction in the in-line force to 87% of the force found in long crested seas have remained a somewhat magic number.

Aage et al. 1989 investigated the distributions of the in-line, the transverse and the resulting force as function of the directional spread. The directional spread was either zero (long crested waves), a $\cos^{2s}(\theta/2)$ spreading function with a constant standard deviation of 29 degrees for all frequencies, or a reproduce North Sea spreading function, which has a minimum spread around the spectrum peak and a large spread of the high frequencies.

In Fig. 39 the curves for the higher in-line forces and the resultant forces for the 2-D and the 3-D waves respectively are nearly identical. This shows that the in-line

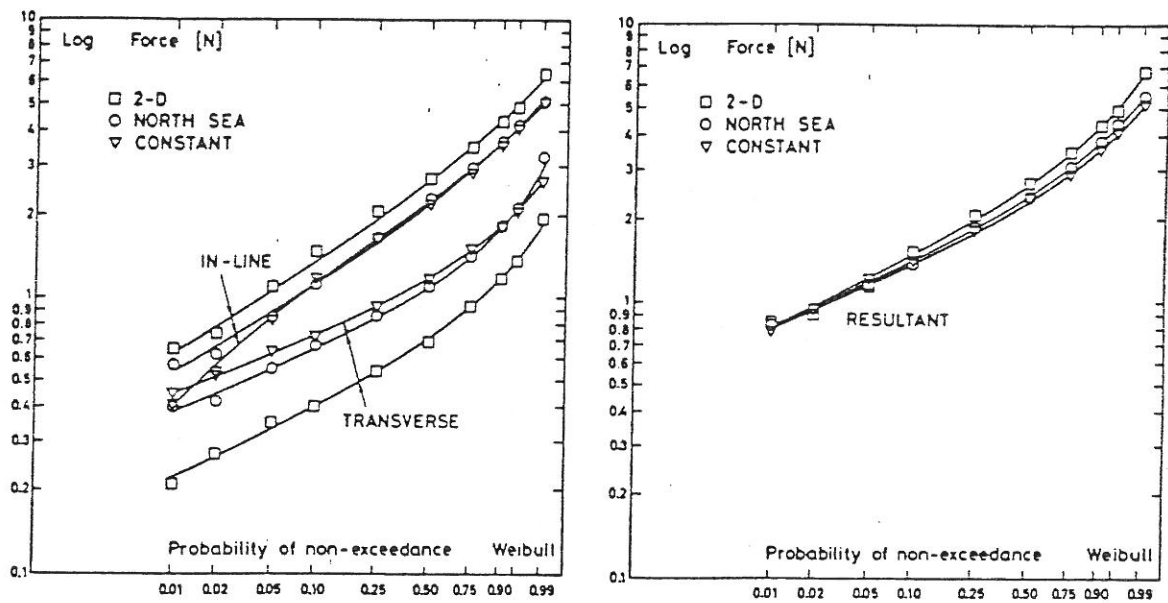


Figure 39: Distributions of in-line, transverse, and resulting forces in waves with different spreading functions. (Aage et al. 1989).

and the transverse forces are generally out of phase. The statistical distributions of the 3-D wave forces do not vary significantly with the two quite different spreading functions tested. The in-line (or resultant) forces in short crested waves are about 85% of the forces in similar long crested waves. However, the transversal forces are about 40-80% larger in short crested waves than in long crested waves.

Fig. 40 a and b show the variation of the ratio of the in-line forces as function of the horizontal level for short crested and long crested waves respectively. Figure 40 b is from a experimental study at University of Aalborg performed with the same cylinder as used by Aage et al., 1989.

It is seen that the ratio between the 3-D and 2-D in-line wave forces is rather independent of the water depth and the significant wave height. Note that Fig. 40-a shows a 90% fractile while Fig. 40-b shows the *RMS* values.

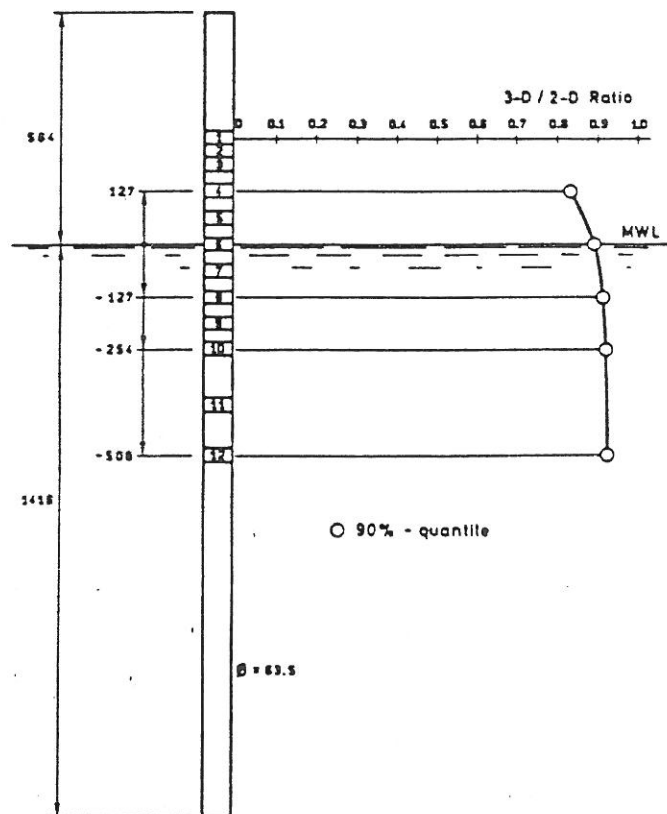


Figure 40: Ratio between in-line forces in short crested and long crested waves respectively.

a) 90% quantile. $H_s = 0.25$ m, $T_p = 2.2$ sec. Waterdepth = 3.0 m
 North sea spreading function on 3-D waves. (Aage et al. 1989)

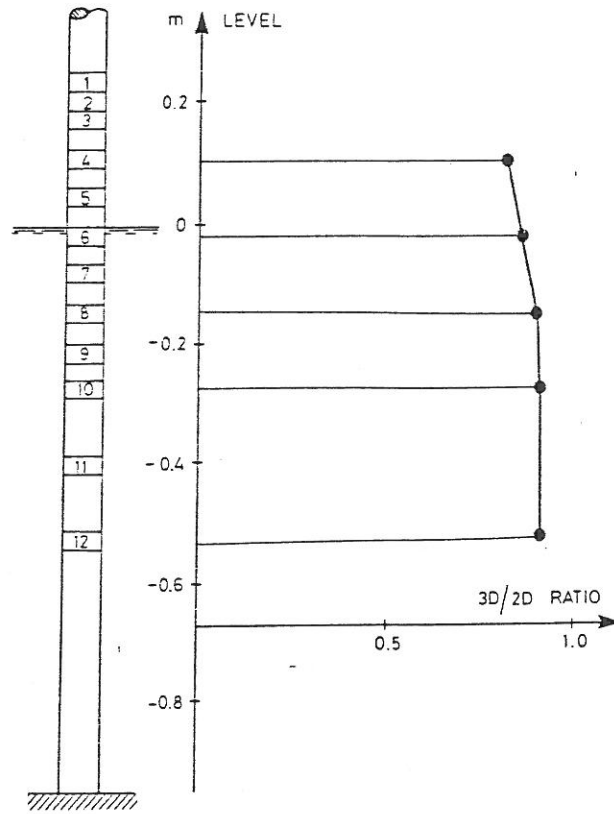


Figure 40: *Ratio between in-line forces in short crested and long crested waves respectively.*

b) Rms values.

$H_s = 0.15$ m, $T_p = 2.2$ sec. Waterdepth = 1.0 m.

\cos^2 spreading function on 3-D waves.

(Frigaard and Burcharth 1988)

Isaacson and Nwogu 1988 calculated the spectral density of the force on a cylinder in short crested waves and compared with measurements. The calculations were based on a linearization of the drag term in Morison's equation.

The linearized spectral density of the in-line and the transverse forces in multi-directional seas were found to be expressed as

$$S_{F_x}(\omega) = \frac{18}{\pi} \sigma_U^2 \left[\int_0^{\pi/2} \cos^2 \theta \sqrt{\cos^2 \theta + \frac{\sigma_V^2}{\sigma_U^2} \cdot \sin^2 \theta} d\theta \right]^2 \cdot \left[\frac{1}{2} \rho \cdot D \cdot C_D \right]^2 \cdot S_\mu(\omega) + \left[\rho \frac{D^2}{4} \cdot C_m \right]^2 \cdot S_{\dot{U}}(\omega) \quad (38)$$

$$S_{F_y}(\omega) = \frac{18}{\pi} \sigma_V^2 \cdot \left[\int_0^{\pi/2} \sin^2 \theta \cdot \sqrt{\cos^2 \theta + \frac{\sigma_V^2}{\sigma_U^2} \cdot \sin^2 \theta} d\theta \right]^2 \cdot \left[\frac{1}{2} \rho \cdot D \cdot C_D \right]^2 \cdot S_V(\omega) + \left[\rho \cdot \frac{D^2}{4} \cdot C_m \right]^2 \cdot S_{\dot{V}}(\omega) \quad (38)$$

where σ_U and σ_V are the standard deviations of the two horizontal particle velocities.

For the unidirectional case formula (38) leads to

$$S_{F_x}(\omega) = \frac{8}{\pi} \left[\frac{1}{2} \rho \cdot D \cdot C_D \right]^2 \cdot \sigma_U^2 \cdot S_U(\omega) + \left[\rho \cdot \frac{D^2}{4} \cdot C_m \right]^2 \cdot S_{\dot{U}}(\omega) \quad (39)$$

Fig. 41 shows an example of the use of (38). It is demonstrated that the formula predicts the in-line force spectra very well.

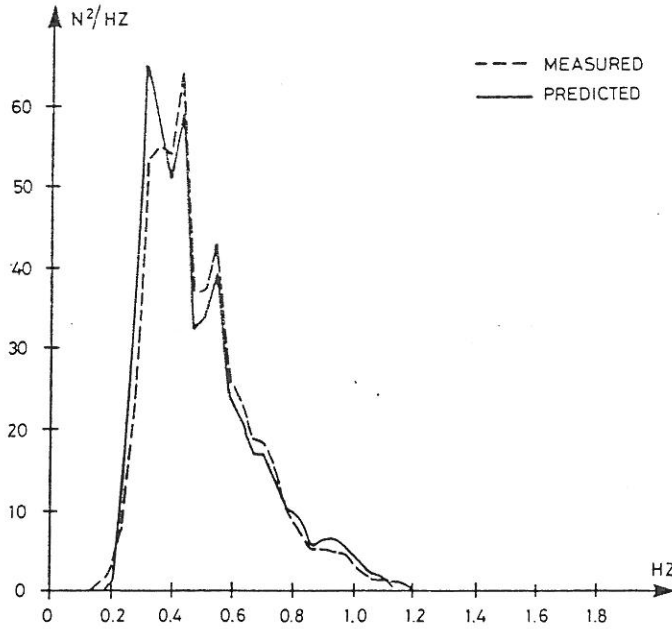


Figure 41: Measured and predicted spectra for the in-line force on a segment 40 cm below MWL.

Short crested waves with spectral peak frequency $f_o = 0.33$ Hz, $H_{m0} = 0.45$ m and cosine spreading function. (Isaacson and Nwogu 1988).

7 Concluding remarks

The presented discussion of the Morison equation is not complete. However, it should be clear that the formula is semi-empirical and many uncertainties^{are} related to its practical use. Especially when used to predict fluid forces on members in "real waves", not only the kinematics of the flow but also the force-transfer coefficients, become increasingly uncertain, see for example Sarpkaya and Isaacson 1981. Consequently the recommendations of various authoritative sources reveal substantial latitude.

It should be noted that this note deals only with wave-generated forces on fixed vertical slender cylinders. Wave forces on flexible cylinders and horizontal cylinders can be very different from what is found for fixed vertical cylinders.

8 References

- Aage, C. et al. : *Wave Loads on a Cylinder in 2-D and 3-D Deep Water Waves*. Proc. of 8th Int. Conf. on Offshore Mechanics and Arctic Engineering, The Hague 1989.
- Bearman, P.W. and Graham, J.M.R. : *Hydrodynamic Forces on Cylindrical Bodies in Oscillatory Flow*. BOSS '79. 1979.
- Bearman, P.W. : *Vortex shedding From Oscillating bluff Bodies*. Ann. Rev. Fluid Mech., pp 195-222, 1984.
- Blevins, R.D. : *Flow-induced vibration*. Van Nostrand, 1977.
- Bostrøm, T. and Overvik, T. : *Hydrodynamic Force Coefficients in Random Wave Conditions*. Proc. of 5th Int. Conf. on Offshore Mechanics and Arctic Engineering. Tokyo 1986.
- Bruun, P. : *Bølger på dypt og grunt vann*. Norges tekniske Høgskole, 1981 (in Norwegian).
- Chakrabarti, S. : *Forces on Vertical Cylinder due to Random Waves*. J. of Waterway, Port, Coastal and Ocean Eng. Vol 114, pp. 267-280. May 1988.
- Cotter, D. and Chakrabarti, S. : *Wave Force Tests on Vertical and Inclined Cylinders*. J. of Waterway, Port, Coastal and Ocean Eng. Vol 110, pp. 1-14. Feb. 1984.
- Dawson, T.H. : *In-Line Forces on Vertical Cylinders in Deepwater Waves*. OTC 4831, Houston 1984.
- Dean, R.G. : *Stream Function Wave Theory: Validity and Application*. Proc. Santa Barbara Conf. on Coastal Eng. 1965.
- Dean, R.G. et al. : *Force Coefficients From Wave Project I and II. Data Including Free Surface Effects*. Society of Petroleum Engineers Journal, Dec. 1981.
- Dean, R.G. et al. : *Wave Forces on a Pile in the Surface Zone from the Wave crest to the Wave Trough*. Proc. Symp. "Separated Flow around Marine Structures". NTH 1985.

- Fredsøe, J. : *Kræfter på cylindre og rørledninger*. Noter til offshore-teknik, Dth 1985 (in Danish).
- Isaacson, M. and Nwogu, O. : *Short-crested Wave Forces on a Vertical Pile*. Proc. of 7th Int. Conf. on Offshore Mechanics and Artic Engineering, vol. II, pp 47-54. Houston 1988.
- Kjeldsen, P. et al. : *Wave Forces on Vertical Piles caused by 2- and 3-Dimensional Breaking Waves*. 20th Int. Conf on Coastal Eng. Taipei 1986.
- Laird, A.D.K. et al. : *Water Eddy Forces on Oscillating Cylinders*. ASCE Transactions Vol. 127 Part 1, 1971.
- LIC Engineering A/S : *Bølgebelastning på cylinder i 2-D og 3-D bølger. Forsøgsbehandling*. Energiministeriet EFP 85. July 1987 (in Danish).
- Morison, J.R. et al. : *Experimental Studies of Forces on Piles*. Proc. 4th Int. Conf. on Coastal Eng. 1953.
- Nielsen, S.R.K. : *Strømningsinducerede svingninger*. Aalborg Tekniske Universitetsforlag 1986 (in Danish).
- Olsen, O. : *Morison's equation - Applications and Limitations*. Norske Sivilingeniørers Forening.
- Sarpkaya, T. : *In-Line and Transverse Forces on Cylinders in Oscillatory Flow at High Reynolds Numbers*. OTC 2533, Houston 1976.
- Sarpkaya, T. : *In-Line and Transverse Forces on Cylinders in Oscillatory Flow at High Reynolds Numbers*. *J. of Ship Reseach*. Vol 21, pp. 200-216, Dec. 1977.
- Sarpkaya, T. and Isaacson, M. : *Mechanics of wave forces on offshore structures*. Van Nostand, 1981.
- Sarpkaya, T. : *Wave Forces on Inclined Smooth and Rough Circular Cylinders*. OTC 4227, Houston 1982.
- Sarpkaya, T. and Storm, M. : *In-Line force on a cylinder translating in oscillatory flow*. App. Ocean Research, Vol 7, pp. 188-196. 1985.
- Shaw, T.L. (Editor) : *Mechanics of Wave-Induced Forces on Cylinders*. Pitman Advanced Publishing Program, London 1979.
- Stansby, P. et al. : *Quasi-2-D Forces on a Vertical Cylinder in Waves*. *J. of Waterway, Port, Coastal and Ocean Eng.*, vol 109, pp. 128-132. Feb. 1983.
- Torum, A. and Reed, K. : *On the Spanwise Correlation of Wave Forces on Slender Structures*. OTC 4226, 1982.
- Torum, A. : *Wave forces on a pile in the surface zone. Regular, non-breaking waves*. Marintek. Report No. 1.9, Dec. 1985.
- Wallingford Hydraulics Research Station : *Wave Loading on a Large Vertical Cylinder in Multi-Directional Random Waves*. Report no. EX 726, April 1976.
- Williamson, C.H.K. : *Sinusoidal Flow Relative to Circular Cylinders*. *J. Fluid Mech.*, Vol. 32, part 1, pp 55-68, 1968.

Yamamoto, T. and Nath, J. : *Hydrodynamic Forces on Groups of Cylinders*. OTC 2499, Houston 1976.